Spring 5-10-2022

HYPERBRANCHED POLYESTER-BASED DRUG DELIVERY SYSTEM FOR THE OPTICAL IMAGING AND TREATMENT OF CANCER

Truptiben Patel
Pittsburg State University, tpatel@gus.pittstate.edu

HYPERBRANCHED POLYESTER-BASED DRUG DELIVERY SYSTEM FOR THE OPTICAL IMAGING AND TREATMENT OF CANCER

A Thesis Submitted to the Graduate School
in Partial Fulfillment of the Requirements
For the Degree of
Master of Science in Polymer Chemistry

Truptiben Patel

Pittsburg State University

Pittsburg, Kansas

May 2022

HYPERBRANCHED POLYESTER-BASED DRUG DELIVERY SYSTEM FOR THE OPTICAL IMAGING AND TREATMENT OF CANCER

Truptiben Patel

APPROVED:

Thesis Advisor _____

Dr. Santimukul Santra, Department of Chemistry

Committee Member _____

Dr. James McAfee, Department of Chemistry

Committee Member _____

Dr. Phillip Harries, Department of Biology

ACKNOWLEDGEMENTS

First and foremost, I would like to express my gratitude to Dr. Santimukul Santra for accepting me as a graduate student in his lab and Dr. Tuhina Banerjee for supporting his decision. I would like to thank them for all the research opportunities, academic guidance, and financial assistant throughout the program. Their knowledge in the field of organic synthesis, polymer chemistry, cancer and infectious diseases research has helped me to become the researcher I am today. They have always encouraged me to pursue my goals and not settle for anything less than my potential, so I am very thankful and grateful for them in pushing my limits and encouraging me towards pursuing Ph. D.

Secondly, I would like to thank the Chemistry department and the Kansas Polymer Research Center for providing the facilities to carry out my projects using instruments such as NMR, DSC, TGA, GPC, etc. Personal thanks to Dr. Jian Hong for training, guiding, and helping in using some of the instruments and analysis. A huge appreciation for the faculty of the department for always encouraging and checking up on me about the progression of the projects and offering guidance if needed. The committee members including Dr. Santra, Dr. James McAfee, and Dr. Phillip Harris for their guidance and support throughout the project. Without their time and energy in revising my thesis and correcting it, I would not have come this far.

Last but not the least, I would like to thank my family back home in India for always being my rock, all the lab members including Paul, Thai, Kajal, Neelima, and Eniola for their steady support. I cannot thank them enough for their emotional, mental, and spiritual support throughout my masters.

HYPERBRANCHED POLYESTER-BASED DRUG DELIVERY SYSTEM FOR THE OPTICAL IMAGING AND TREATMENT OF CANCER

An Abstract of the Thesis by
Truptiben Patel

Hyperbranched polymers are a promising new drug delivery system for biomedical applications. In this research, a novel hyperbranched polyester polymer was synthesized using melt polymerization and utilizing our proprietary A_2B monomer, triethylene glycol and diethylenetriaminepentaacetic acid (DTPA). This polymerization process was catalyzed by p-toluene sulfonic acid and was monitored by analyzing the polymer sample at regular time intervals. The final polymer was purified using the solvent precipitation method and characterized using MALDI-TOF, NMR, and GPC, DSC, TGA, FT-IR. The solvent diffusion method was used to formulate the polymeric nanoparticles which will be used to encapsulate the drug doxorubicin. The "Click" chemistry method was used to decorate the nanoparticle surface with folic acid for targeted drug delivery. The efficiency of this drug delivery system was monitored and analyzed by performing cell-based assays such as MTT assay, ROS study, migration assay, apoptosis, necrosis, comet assay, and drug release study. Non-small cell lung cancer (NSCLC) cells were used as a model cancer cell line in these tests.

Keywords: Polyester · Biocompatible · Biodegradable · Nanoparticle · Cancer · Nanomedicine · Targeted Delivery · Optical Imaging

TABLE OF CONTENTS

LIST OF FIGURES

Figures *Page*

LIST OF SCHEMES

Schemes *Page*

Chapter I

Literature Overview

Cancer Background:

According to the American Cancer Society, lung and bronchus cancer stands at the top in mortality rate in both men and women. From reported cases of lung cancer, more than 50 percent of cases ends with death in both sexes. (1) The statistical analysis of the probability of developing invasive cancer during selected age intervals by sex shows that lung and bronchus cancer comes second after breast cancer with probability of 1 in 59 and 1 in 17 in the age group 60-69 and 70-older respectively. (1) The major risk factor for developing lung cancer is cigarette smoking which accounts for 80 percent of lung cancer deaths. (1) Lung cancer is divided into two main categories: non-small cell lung cancer (NSCLS), and small cell lung cancer (SCLC). NSCLC accounts for 9 out of 10 cases and has a slower growth rate compared to SCLC. Due to its slow growth rate, this type of cancer is typically diagnosed when it has already reached an advanced level. The treatment options include surgery, chemotherapy, hormone therapy, targeted drugs, immunotherapy, and/or radiation therapy. (2) Among all treatment options available, targeted drug therapy is becoming more popular due to the flexibility of the treatment. Unlike chemotherapy, targeted drug therapy shows both, promising results in reducing cancer cells while also having minimal effect on healthy cells. Another advantage of targeted therapy is that the side effects are not as severe as other therapies. There has been a large amount of research

done on targeted drug therapy which can also be called personalized medicine/precision medicine because of its target specificity for cancer cells. (3) The technological advancement in this area allows us to go to the nano level to treat the cancer which eventually becomes personalized nanomedicine. The area of personalized nanomedicine is a diverse field with a ton of flexibility in choosing drugs, drug carriers, drug delivery systems, monitoring the treatment, etc. When it comes to an efficient drug delivery system, nanoparticles always come first due to flexibility in synthesis, functionality, and chemical properties. Nanoparticles are globular shaped, submicron-sized structures which can be synthesized using a polymer, lipids, micelles, or metals. (3)

History of Polymer:

Polymers are believed to have existed since before the origin of life on earth over 3 billion years ago. Our bodies have been relying on natural polymers such as DNA, RNA, proteins, and carbohydrate since the beginning and today, we are surrounded by polymers in everyday life. Polymers can be defined as a chain of repeating blocks called monomers. (4,5) The founding father of the polymer science, a German chemist named Dr. Hermann Staudinger, spent three decades in groundbreaking research about polymer structures and won a Nobel Prize in 1953 for his excellent work. Staudinger's discovery of macromolecules and their biological applications lie at the root of the discipline of polymer science. If it wasn't for his efforts, it would have taken a long time for polymer science to grow and expand further. (6) Groundbreaking research by Carothers advanced the first age of polymers followed by Karl Ziegler in the second age of polymers and Dr. A. MacLachlan in the third age of polymers. These scientists led, modified, and advanced the polymer science which we study today. Due to their expertise, polymers can be

studied and categorized based on their discovery timeline, backbone monomers and structural properties. (4-6)

Natural polymers have been abundant since the beginning of a life and provide us today with the resources for the creating advanced synthetic polymers. The era of natural polymers can be classified as a "precursor age" that has led to the manufacture of man-made polymers. The birth of synthetic polymer chemistry happened after the discovery and manufacturing of Bakelite and the "plastics age" became a key feature of the 20th century. The first age of polymers includes the discovery of rubbers which have a rich and complex history all around the world. The discovery of cellulose ester is another milestone during the first age of polymers followed by Bakelite. The time from 1910-1930 was truly an excellent period for industrial advancement with the discoveries of linear polymer such as polyvinyl chloride (PVC), polystyrene, polyethylene (PE), polypropylene (PP), and Teflon, etc. The second age of polymers advanced the manufacturing of PE and PP to make it more user friendly, environment friendly, and cost effective. The years from 1940-1970 were significantly beneficial and substantial in the expansion of manufacturing industries for synthetic polymers. The third age of polymers allows us to use low-cost, high-performance polymers in our everyday life. (6)

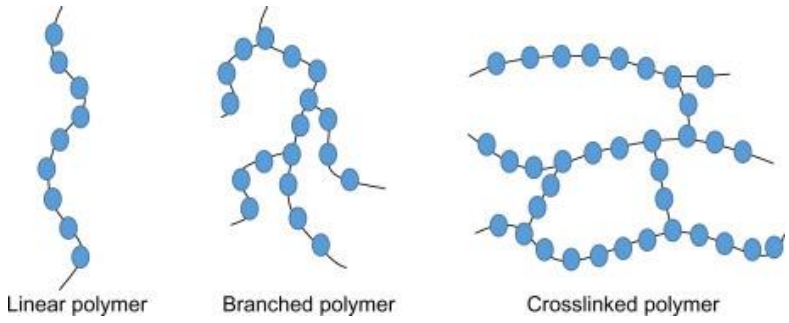

Figure 1: Schematic representation of different types of polymers (7)

Polymers can be classified based on their structure which can be linear, branched, or cross-linked. Linear polymers are long chains of monomer units which are arranged in A-B-A-B-, A-A-B-B-, or A-B-B-A-A-B-A-. Linear polymers are usually synthesized using addition polymerization where the monomer molecules arrange in continuous or alternate pattern to form a long chain. (8) Polymers such as PVC, PEG, PLGA, PLA are classic examples of linear polymers. When it comes to linear polymers for drug delivery, Robert Langer's name must be recognized for his discoveries since 1980s. His research on polymeric delivery systems advanced the stream of targeted therapeutics. Langer worked on polymers such as poly (hydroxyethyl methacrylate), ethylene-vinyl acetate, polyacrylamide, and poly (vinyl pyrrolidone) to advance the polymeric drug delivery systems. (10, 11, 12) PEG is one of the major polymers used for drug delivery due to its water solubility, biocompatibility, low toxicity, etc. Studies have shown that PEGylated drug delivery systems have higher blood circulation time, stability of drugs, and easy renal clearance due to its size and low molecular mass. (13) Another FDA approved polymer is PLGA which has been used widely for biological applications. PLGA drug delivery systems have shown exceptional results when it comes to wound healing, incorporating drugs such as curcumin which has poor solubility. (14) Having all these advantaged of linear polymers, there are still some drawbacks which can be overcome in the future. Having a linear morphology, the encapsulation and conjugation of cargos become challenging which leads to minimum drug loading capacity (for example ~1% in PLGA drug delivery systems). The aggregation of polymers in the acidic

environment of cancerous tumors is another issue that can be explored to improve drug delivery systems. (14)

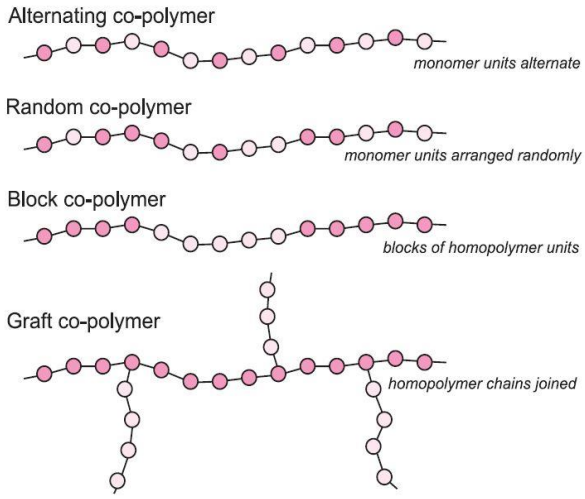

Figure 2: Structure of different types of co-polymers. (9)

Branched polymers can be divided into two categories: hyperbranched and dendrimers. Hyperbranched polymers tend to have monomers that are AB_2 ($x \geq 2$) type which results in globular shape with multiple functional groups on the surface. Polyglycerol, polyether are examples of hyperbranched polymers. Dendrimers such as polyamidoamine (PAMAM) are widely used in biological applications. Compared to hyperbranched, dendrimers are more uniform structurally resulting in a star shape with multiple functional groups on the surface. Due to its uniformed structure, the synthesis of dendrimers is more challenging than hyperbranched. (15) Lastly, cross-linked polymers have similar monomer molecules as branched polymers, and these molecules form a strong covalent bond within. Bakelite and melamine are examples of cross-linked polymers. Furthermore, depending on the monomer, polymers are differentiated into homomer and co-polymer. Homomers have only one monomer unit, either A_2 or B_2 type, which forms an entire polymer. Whereas co-polymers contain different types of monomers such as the A_2B or AB_2 types.

(16) Linear polymers have been very beneficial in industrial applications whereas branched polymers have been widely used in biological applications such as drug delivery. (17)

Implication of Branched polymers in drug delivery:

Dendritic polymers have been used for biological applications due to their unique structural characteristics which has allowed the drug delivery systems to go from macro to micro to nano scale. The dendritic polymers are classified into perfectly branched dendrimers and imperfectly branched hyperbranched polymers or HBPs based on the architecture. Both types of dendrimers resemble similar tree-like arrangement but, the topological arrangement makes them unique from each other. (18) The first dendrimer, poly(amidoamine) (PAMAM), was introduced by Tomalia in 1980s along with its first use in biological applications. The dendritic polymers acquire structural characteristics such as a multi-functional core, surface groups, and branching units. One characteristic which sets them apart from other linear polymer is the ability to mimic the size of nanoscale proteins such as insulin (smallest protein) and histone (large protein) which varies from 2-15nm. Furthermore, dendritic polymers have qualities as listed which makes them an exceptional candidate for the biological applications such as drug delivery: i) branched structure with multiple functional groups and cavities to carry multiple cargoes in one molecule of polymer, ii) controlled multifunctional structure, iii) biocompatible which benefits substrate/ligand binding receptor, vi) easy to tune characteristics such as size, surface potential, and number of peripheral functional groups, etc. (4)

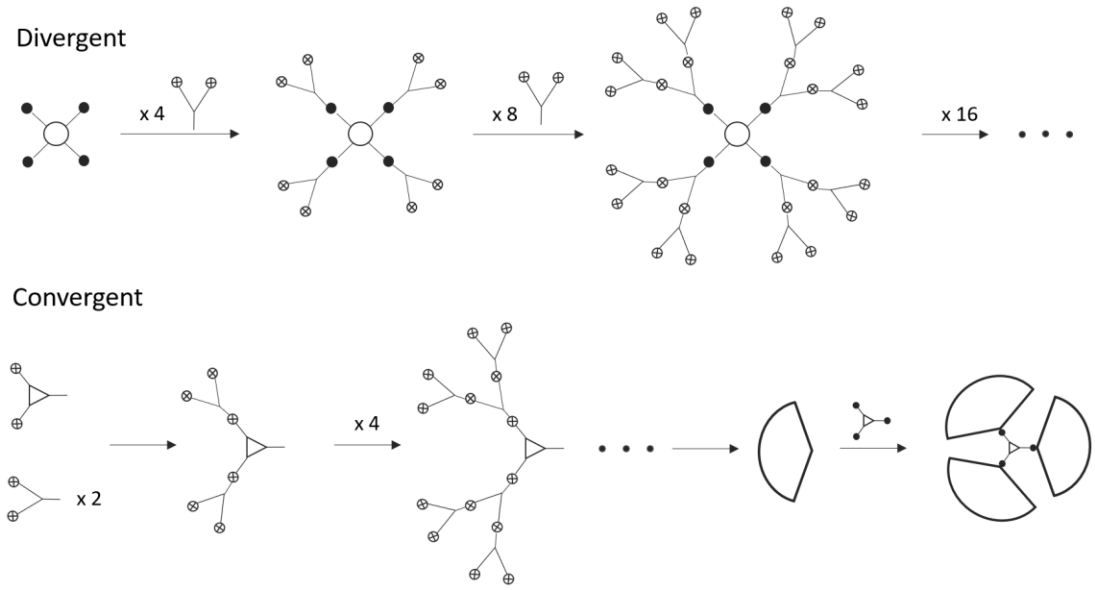

Figure 3: Two synthetic approaches of dendrimers: divergent and convergent (19)

Having similar characteristics, dendrimers and HBPs have different synthetic approaches and molecular arrangement that make them unique. Dendrimers are synthesized stepwise following either divergent or convergent growth. Divergent growth starts from the core of the polymers and goes towards the periphery from generation to generation. The formation of every generation results in doubling the molar mass which is useful in synthesizing large molecular weight polymers. However, divergent growth can lead to incomplete branching and side reactions and the purification of polymer becomes challenging and tiresome. (18) On the other side, the convergent approach starts from the periphery and goes towards the core by growing monomers large enough and attaching them to the appropriate core. The purification of polymers is easier than divergent growth with simple and easy steps. Both multi-step synthetic approaches result in globular, tree-like structure with multiple cavities within the structure where either hydrophobic or hydrophilic molecules can be conjugated and encapsulated for biological applications. (18)

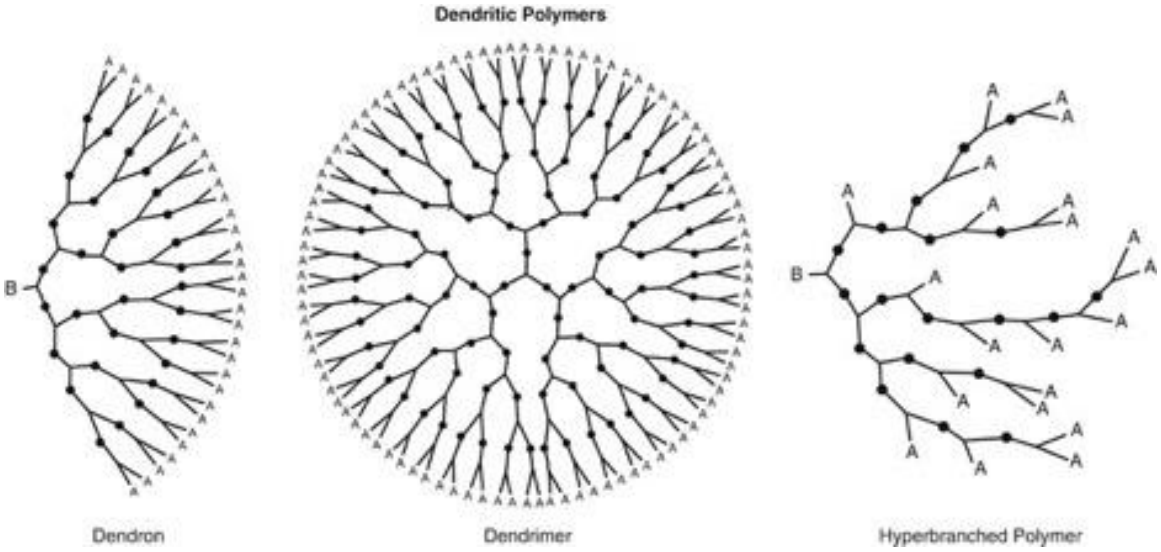

Figure 4: Various types of dendritic polymers and their structures (29)

Different from dendrimers, HBPs are synthesized in one-step, one-pot condensation reactions utilizing AB_2-type monomers. Since the branching is not uniformed in HBPs, the polydispersity is relatively high, but it can be controlled during the synthesis with the reaction order of monomer units. Such methods include activation of B group after the reaction of A group, slow addition of monomer and subsequent anionic polymerization. Among previously studied aliphatic HBPs such as polyglycerols, polyethers, and polyesters, most of the reported HBPs were utilizing aromatic rings until a novel aliphatic hyperbranched polyesters (HBPE) was synthesized utilizing AB_2 and AB_3 monomers based on diethyl malonate by Dr. Santra and Dr. Kumar. This new family of HBPE was easy to synthesize and purify, with higher yield, a multifunctional surface, as well as efficient bioconjugation and encapsulation for drug delivery. The advantage of having polyester in the backbone makes the polymer more biocompatible since it can be degraded by the esterase enzyme available in the cellular environment. Continuing their interest in HBPE, Santra and collogues developed the very first HBPE utilizing hydrophilic surface with hydrophobic cavities for the formulation of multifunctional drug delivery tool in the treatment of A549 NSCLC cells. The intriguing results showed low cytotoxicity towards healthy cells with effective killing of cancer cells.

These polymers exhibit exceptional qualities in the formulation of nanoparticles and targeted drug delivery. (16,17)

Nanoparticles: a nanotheranostic tool for the targeted drug delivery:

Nanoparticles are solid, colloidal particles which vary in size on a nanoscale from 2-200 nm. The characteristics such as size, surface potential, UV absorption, and biocompatibility make them an outstanding vehicle for targeted drug delivery. (20) The conventional treatments for cancer such as surgery, chemotherapy, and radiation therapy have a higher cytotoxicity towards the healthy cells and tissues due to non-target specificity. The side effects caused by these treatments such as fatigue, hair loss, headaches, vomiting, seizures, infection, nausea, anemia, fertility problems, etc. can be reduced to a minimum level by using nanoparticles in targeted drug delivery. (1) The main purpose of using nanoparticles for drug delivery is to reduce the cytotoxicity of the drugs on healthy cells and tissues and increase the retention time in the blood for positive effect on tumorous cells. Nanoparticles can be modified using different surface conjugation chemistries such as EDC/NHS, CDI chemistry, and DCC coupling to make them more host-friendly and multifunctional for the successful treatment. The basic structure of nanoparticle can be broken down into three parts: i) the core which is made of polymer, inorganic material such as metals, and lipid, ii) the shell surrounding the core which has cavities to carry the cargos for the drug delivery, and iii) the surface which is modified using surface chemistries to result in multifunctional layer of polymers, surfactant, metal ions, ligands, etc. The core decides the type of nanoparticle whereas the shell and the surface layers decide the type of cargos for encapsulation and the type of cancer cells to target respectively. There are three main types of nanoparticles: a) polymeric, b) inorganic, and c) lipid-based NP. (20,21)

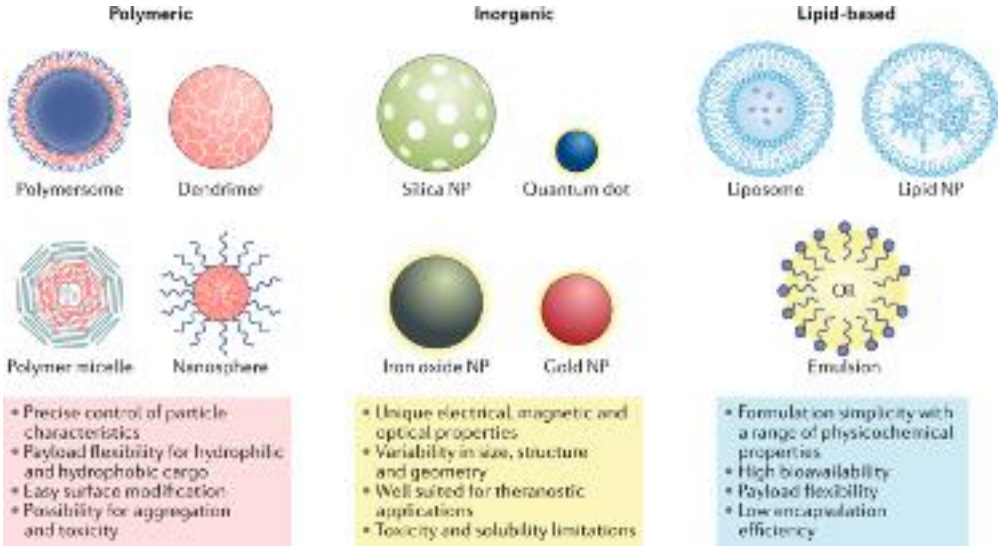

Figure 5: Various types of nanoparticle systems with some of the most common highlighted features and numerous broad advantages and disadvantages regarding cargo, delivery, and patient response. (30)

a) <u>Polymeric nanoparticles:</u>

There are a widely variety of polymeric nanoparticles developed throughout the history of nanomedicine for cancer. The most well-known polymer for therapeutics is PAMAM dendrimer which has been used for multiple cell lines including human epithelial carcinoma cells (KB cells), NSCLC cells (A549 cells), ovarian and breast cancer cells. The findings in all these experiments showed successful targeting through fluorescence microscopy and reduced cytotoxicity. (22) The well-defined structure of dendrimers allows to formulate multifunctional nanoparticles; however, the synthesis of a perfect dendrimer seems challenging. As an alternative, hyperbranched polymers have been used due to their feasible synthesis. Santra et al. discovered a new family of HBPE polymers where multiple cancer cells such as lung, breast, and prostate were targeted with multi-model functionalized nanoparticles utilizing drugs such as doxorubicin, paclitaxel, fingolimod, etc. The results showed an exceptional biocompatibility and biodegradability due to the polyester backbone followed by reduced cytotoxicity and successful cell killing. (16,17)

b) Inorganic nanoparticle:

Inorganic nanoparticles utilize metals in the core such as iron oxide, gold, silver, cerium oxide, silicon, etc and often called metallic nanoparticles. (21-25) Each metallic core contains unique characteristic such as magnetic relaxation (MR) contrast of iron oxide nanoparticle (IONP) allows to monitor the treatment through MRI scan (21), surface plasmon resonance (SPR) of gold nanoparticle (GNP) allows to monitor treatment through its optical, photothermal, and binding properties with organic molecules and results in reduced cytotoxicity (23). Cerium oxide as a core of nanoparticle has a synergistic effect in the production of reactive oxygen species (ROS) which can be monitored through fluorescence microscopy and its small diameter helps to pass the blood-brain barrier (BBB) (25). There has been a plethora of research done on metallic nanoparticles where the shell has been modified by adding chelating agents and targeted to specific ligands. Findings suggested that metallic nanoparticles could be the next tool for not only targeted cancer therapy but also for the neurogenerative disease treatment.

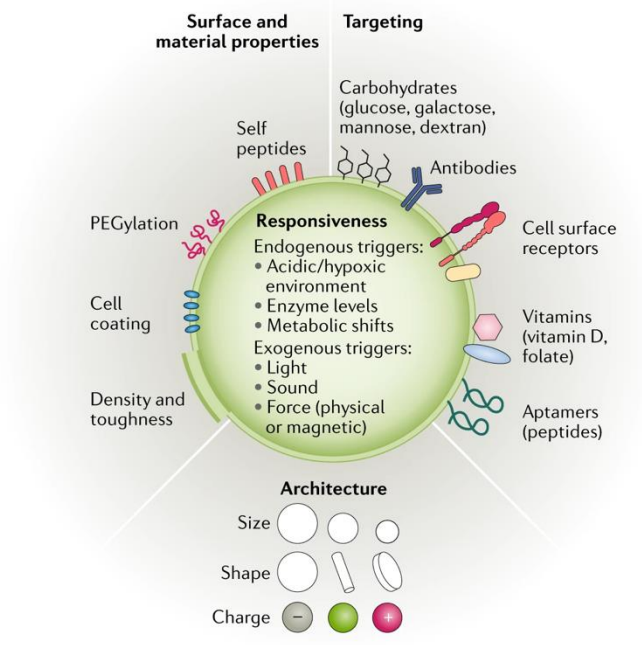

Figure 6: Commonly engineered nanoparticle surface properties that allow for enhanced delivery. (30)

c) Lipid-based nanoparticle:

Lipid based nanoparticles are known liposomes. The liposomes are vesicles which are formed when two phospholipid molecules come together, and their bilayers form a vesicle by trapping the fluid inside. The cargos can be entrapped where the fluid is and can be delivered successfully to the targeted cells due to their excellent biocompatibility and biodegradability. The liposomes are flexible for the surface conjugation using ligands or polymer for the targeted delivery. (28)

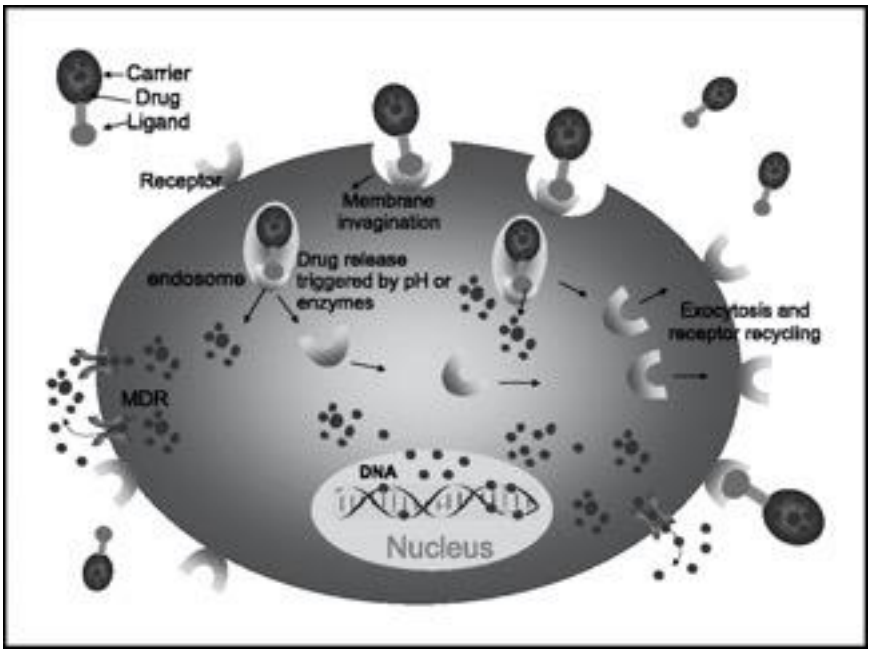

Figure 7: Internalization of nanoparticles via receptor-mediated endocytosis. Tumor-specific ligands or antibodies on the NPs bind to cell-surface receptors, which trigger internalization of the NPs into the cell through endosomes. As a pH value in the interior of the endosome becomes acidic, the drug is released form the NPs and goes into the cytoplasm. (31)

To determine if the efficacy of functionalized nanoparticles, biological assays such as cell internalization, cytotoxicity assay, and apoptosis and necrosis assay can be performed. The cell internalization assay uses two types of dyes where the nucleus and cytoplasm are stained to

observe the morphology under fluorescence microscopy. The cytotoxicity assay, also known as the MTT assay, shows the percent viability of cells after the treatment which helps to determine the target specificity and drug loading in the cancer cells. Apoptosis and necrosis assays determine the cell death time which becomes an important aspect in clinical trials.

In summary, the diagnosis and treatment options for cancer has been an intriguing field with plenty of research and case studies. The treatment options keep improving everyday but so does the number of cases and deaths. With the help of targeted therapy using polymers, we could improve the current treatment options and prevent patients from going through the ugly deformation caused by traditional treatments. Polymers seem a very promising options, especially branched polymers, in targeted therapy which we have proposed in the next chapter.

Chapter II

Introduction

Cancer has been one of the leading causes of death globally, especially lung and bronchus cancer. According to the statistical analysis by the American Cancer Society, lung and bronchus cancer cases results in more deaths than any other types of cancer. The major causes of lung cancer such as smoking, tobacco, and exposure to environmental carcinogens, play a primary role not only for a person who smokes or chews tobacco but also for the people around them are at an increased risk of getting cancer. (1) Lung cancer is categorized into two types: NSCLS which grows slowly and is challenging to detect at early stage and SCLS which grows quickly. (2) Traditionally, surgery is the preferred treatment option for early-stage cancer, but chemotherapy and radiation therapy play a major role when the cancer has metastasized. (1) The advancement in all these treatments still needs an improvement which can be achieved through targeted therapy and personalized medicine. The advancement in nanomedicine has allowed the delivery of drugs such as Doxorubicin and Paclitaxel with reduced cytotoxicity on healthy cells which is an obstacle in chemotherapy and radiation therapy. (23, 25, 26) Nanomedicine provides the platform to deliver the cargo only to tumor cells through targeted nanoparticle system without harming healthy cells. The characteristics such as flexible surface conjugation, lower cytotoxicity, biocompatibility, and biodegradability make nanoparticles an outstanding candidate for the targeted therapy. There are various options to formulate a nanoparticle such as polymer, metals, lipids, and micelles. (21) Polymers have shown promising results as a drug delivery system

due to their multi-functional groups and amphiphilicity which allows them to encapsulate various drugs, and easily biodegrade. The hyperbranched polyester (HBPE) polymers have been used in various research as a drug delivery system and showed promising results in target specificity, lower cytotoxicity, and biodegradability. (17, 18, 28)

In this study, we developed a novel hyperbranched polyester polymer from a proprietary A_2B monomer and triethylene glycol incorporating DTPA through a melt polymerization reaction, catalyzed by p-TSA. The triethylene glycol provides the hydrophilicity due to the polar groups and provides more space for the encapsulation of cargos. The DTPA acts as a chelating agent which releases the encapsulated drugs only after entering the tumorous microenvironment. Also, the incorporation of DTPA with gadolinium (Gd) allows to monitor MR imaging by giving us T1 and T2 relaxation however, the focus of this study is for the optical imaging. The resulting polymer contains carboxylic functional groups in the periphery which are flexible to conjugate target specific ligands such as folate amine for targeting A549 cell line. The surface conjugation chemistry allows the polymer to stay stable in water in a form of nanoparticle. The polymer was further turned into a functional polymeric nanoparticle by encapsulating Doxorubicin through solvent diffusion method and encapsulating folate amine through EDC/NHS and “Click” chemistries. To compare the target specificity of the functional Doxo-Fol NP, a negative control nanoparticle was synthesized by encapsulating Doxorubicin into a polymeric solution which resulted in Doxo-NP with carboxylic groups on the periphery. The efficacy of both NPs was tested on NSCLC cell line, A549, through various experiments such as cell internalization, cytotoxicity study, apoptosis and necrosis assay, ROS study, migration assay, drug release study, and comet assay.

Results and Discussion:

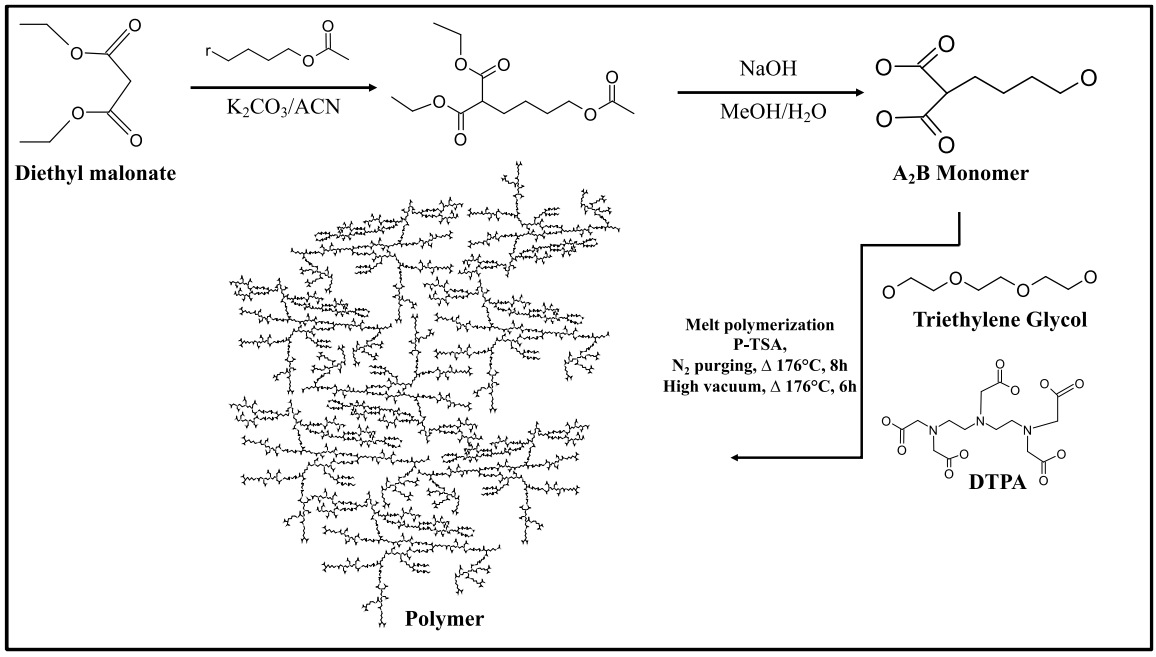

Scheme 1: Schematic presentation of synthesis of hyperbranched polyester polymer

Hyperbranched polyester (HBPE) polymers are widely used for drug delivery due to the exceptional biocompatibility and biodegradability. Here, we have synthesized a sixth generation HBPE incorporating hydrophilic triethylene glycol and DTPA to create an amphiphilic HBPE. The addition of trigol expands the options of choosing drugs due to its hydrophilicity and DTPA makes the polymer dual modal due to its magnetic relaxation properties. The synthesis of the novel HBPE is demonstrated in Scheme1. The starting material, our proprietary A_2B monomer is synthesized as previously reported and characterized by NMR, FT-IR, and GPC methods. The triethylene glycol and DTPA are purchased commercially and characterized using NMR, FT-IR, and GPC methods. To synthesize proposed HBPE polymer, monomer, trigol and DTPA were used in a 1:1:0.1 molar ratio with a catalytic amount 100:1 of p-TSA. The excess moisture was removed from the mixture of all

reactants using high vacuum and UHP N_2. The p-TSA catalyst was added in a ratio mentioned before. The RBF was purged with high vacuum and UHP-N_2 for few times at room temperature and a steady flow of UHP-N2 was supplied at 140 °C-170 °C for 8 h with continuous stirring. After 8 h, a medium vacuum is introduced for 30 min to remove any excess moisture from the RBF and then high vacuum is applied for the polymerization to continue for 6 h. This step results in formation of a high molecular weight polymer from low molecular weight monomers during the heating process. The resulting polymer was purified using mixed solvent precipitation method (DMSO/DI-water). The polymer was dissolved in DMSO and precipitated in water by centrifugation and dried overnight under medium vacuum oven at 40 °C. The final polymer was highly viscous, amber in color, and soluble in methanol, dimethyl sulfoxide, tetrahydrofuran, chloroform. These characteristics showed a successful incorporation of trigol and DTPA into the monomer to achieve the desired polymer. The polymer was characterized using numerous assays such as NMR, FT-IR spectroscopies, GPC, TGA, DSC, and MALDI-TOF.

The ^{1}H-NMR spectra of A_2B monomer, triethylene glycol, and the HBPE polymer are shown in Figure 8. The aliphatic protons in the A2B monomer can be seen from 1.26 – 1.7 ppm (peaks 2 – 4) which shift downfield after from 1.3 – 2.3 ppm (peaks 1 – 3) in the resulting polymer. The protons next to the hydroxyl group and carbonyl group in A_2B monomer are seen at 3.35 (peak 5) and 3.15 (peak 1) ppm respectively which results in downfield shift in the polymer at 4.03 (peak 6) and 3.63 (peak 5) ppm respectively. The ^{1}H-NMR spectrum of triethylene glycol shows aliphatic protons near to hydroxyl group and carbonyl group at 3.5 and 3.4 ppm respectively which results in a downshift at 3.63 and 4.22 ppm respectively in the polymer. The DTPA incorporation can be seen in the spectrum of polymer representing peaks 4 and 5 in Figure 8. This spectrum confirms a successful incorporation of triethylene glycol and DTPA into the polymer backbone.

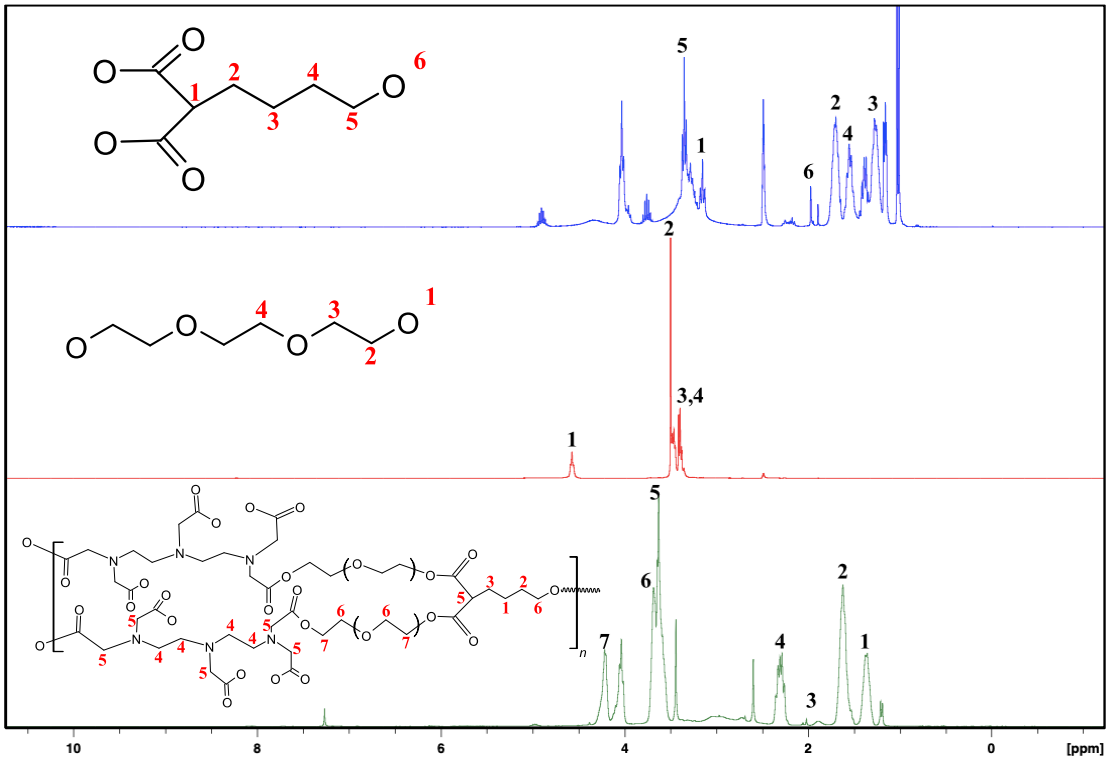

Figure 8: ^{1}H-NMR spectra of A_2B monomer, Trigol, and Polymer respectively

The ^{13}C spectra of A_2B monomer, triethylene glycol, and HBPE polymer is shown in Figure 9. The aliphatic carbons in the A_2B monomer can be seen from 23.92 – 32. 55 ppm which are observed in the polymer as well as a peak 1. The carbon next to hydroxy group and carbonyl carbon can be seen at 62.55 (peak 6) and 171 (peak 1) ppm respectively which results in downshift in the polymer as peaks 5 and 6. The three types of carbon in triethylene glycol can be seen at 60. 69 ppm (peak 1), 72. 75 ppm (peak 2), and 70. 20 ppm (peak 3) which down shifts in the spectrum of polymer as peaks 5, 4, 3 respectively. The incorporation of DTPA was observed at peaks 2 and 6 successfully. The collection of the ^{1}H-NMR and ^{13}C-NMR spectra of DTPA was a challenge due to the acidic groups associated with DTPA which required a basic deuterated solvent for the NMR spectra. Dissolving the DTPA into the usual deuterated solvents such as DMSO-d6, $CDCl_3$, D_2O did not result in collecting an NMR spectrum, so the literatures were used to collect the NMR spectra to confirm a successful incorporation of DTPA for the NMR spectroscopy.

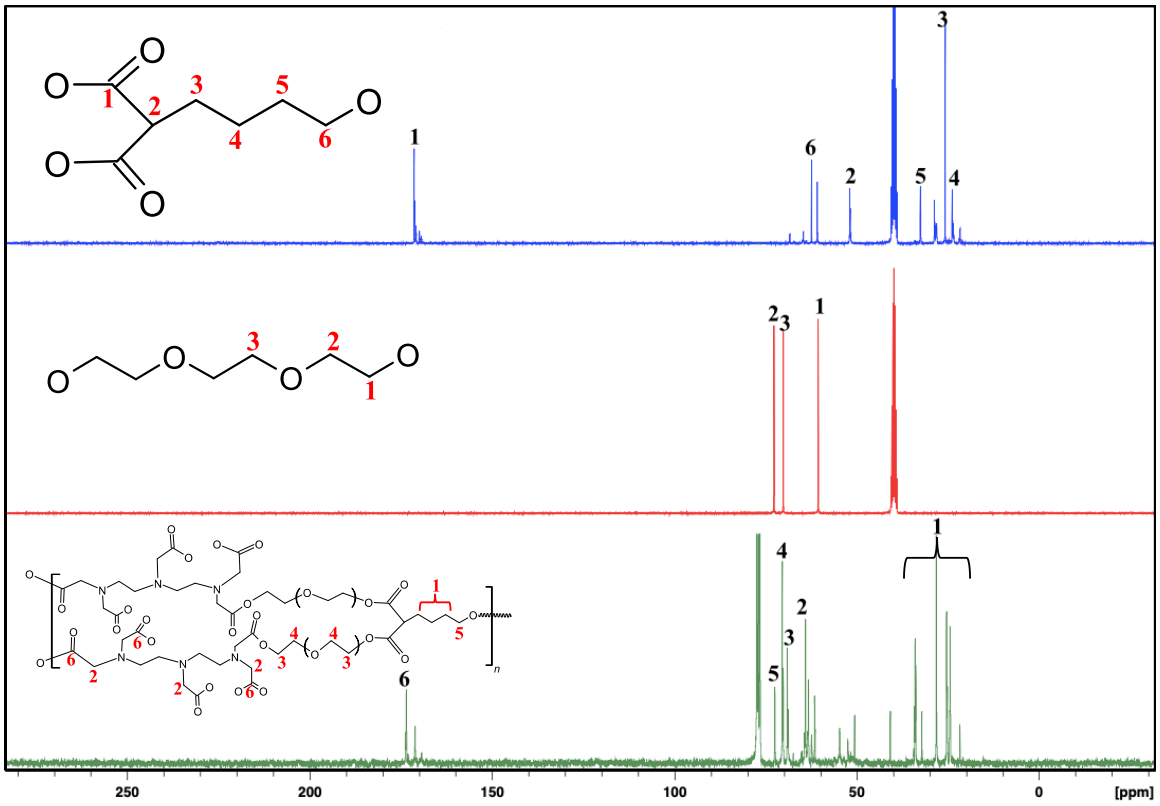

Figure 9: ^{13}C-NMR of A_2B monomer, Trigol and Polymer respectively

The FT-IR spectra of A2B monomer, triethylene glycol, DTPA, and HBPE polymer are shown in Figure 10 (A). The A2B monomer shows a strong carboxylic peak at 1715 cm-1 which shifts to 1730 cm-1 as the ester bond forms during the polymerization. The peaks at 1160 cm-1 and 1106 cm-1 represents the aliphatic ether groups in triethylene glycol. The sharp peaks between 2867 – 2966 cm-1 represents the aliphatic -CH_2 groups associated in each material. An obvious hydroxyl group can be seen at 3400 cm-1 in the monomer, trigol and polymer.

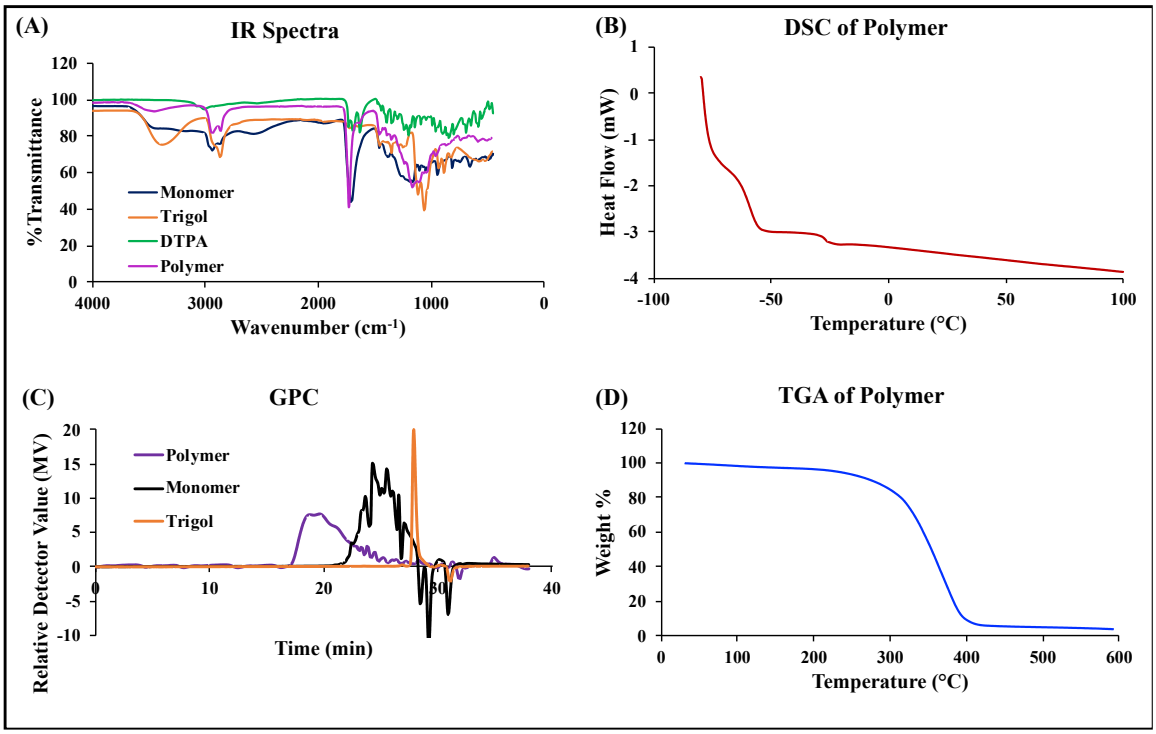

Figure 10: (A) FT-IR spectra of A2B monomer, Trigol, DTPA, and Polymer; (B) DSC curve of Polymer; (C) GPC chromatograms of A2B monomer, Trigol, and Polymer; (D) TGA chromatogram of Polymer.

The TGA of the polymer is sown in Figure 10 (D). A 5% degradation was observed at 230.5 °C which is the evaporation of water left in the polymer. A 10% degradation was observed between 265-270 °C which demonstrated the degradation of the ester bond. The polymer degrades up to 95% by 400 °C which assures the stability of the polymer at physiological conditions. The DSC profile of the polymer in Figure 10 (B) shows a glass transition temperature (Tg) at -70 °C followed by a melting temperature at -22 °C which informs that the polymer is viscous at a room temperature. The GPC profiles of monomer, trigol, and polymer in Figure 10 (C) shows that the retention time of the polymer is very low which contributes to formation of a high molecular weight polymer (Mw = 46,740 Da, Mn = 32,235 Da, PDI = 1.45) eluted in 17-23 min. The monomer comes out through the column as soon as the polymer ends with a tiny overlap and trigol comes at the end being the smallest molecular weight. To determine the quantitative

value of the molecular wight of the polymer, MALDI-TOF is shown in Figure 11. The sample was prepared by co-crystalizing the polymer in a matrix solution containing TA30 and 2.5-dihydroxybenzoic acid and the spectrum was obtained using “Flexcontrol” by Bruker. The molecular wight of the polymer was determined to be 32,650 with small fragments of the oligomers with the molecular weight of 19073.847, 12684.363, and 7504.194 Da.

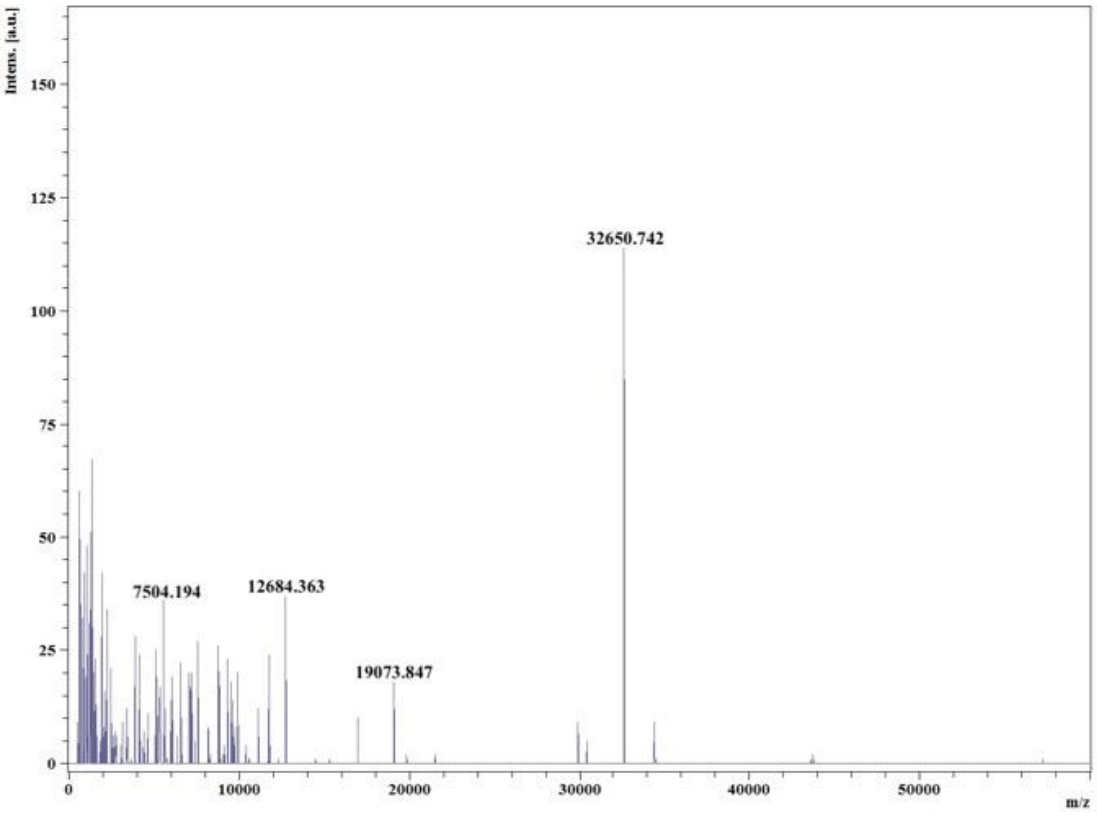

Figure 11: MALDI-TOF chromatogram of polymer

Polymeric Nanoparticle formulation and drug encapsulation:

After confirming a successful characterization of HBPE polymer through characterization techniques, the polymer was formulated into a functional nanoparticle. The formulation of the functional nanoparticle is shown in the Scheme 2.

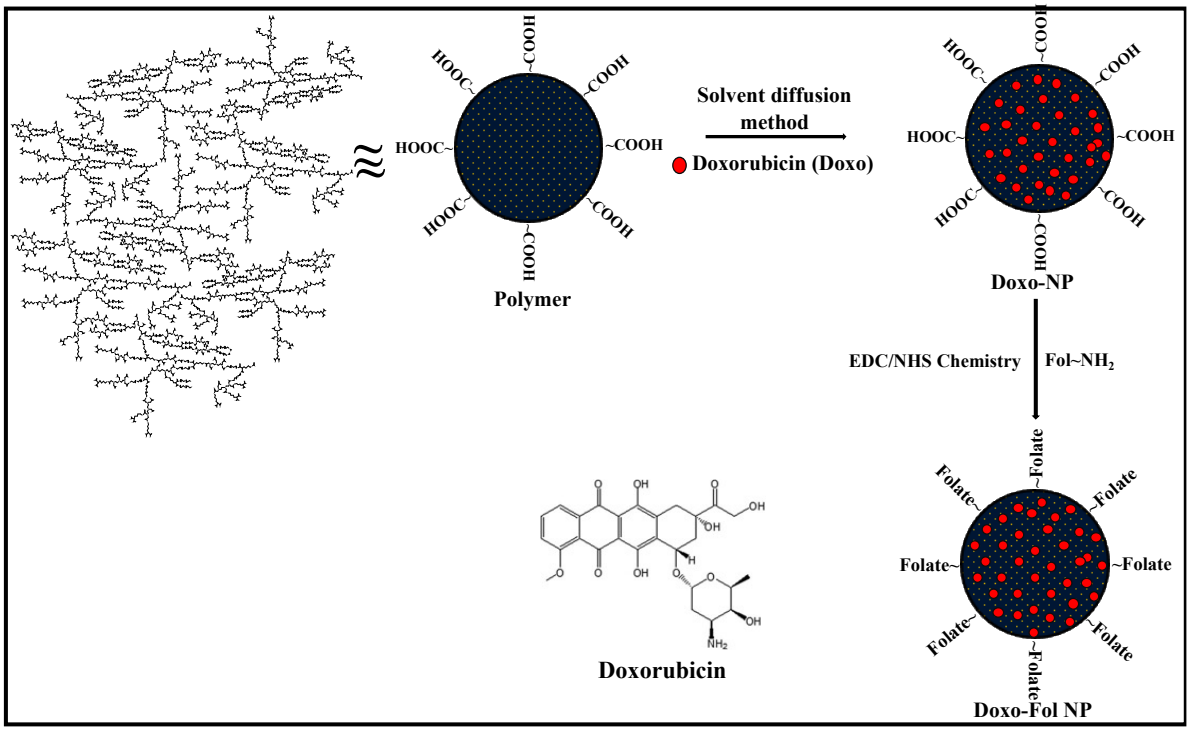

Scheme 2: Schematic presentation of encapsulation of Doxo and conjugation of folic acid

To begin with, a polymeric solution in DMSO was prepared (30 mg/250 µL) and 5 µL doxorubicin drug (10 mg/mL) was added to the polymeric solution slowly with a gentle vortexing. To form a nanoparticle, the polymer solution with doxorubicin was added into a deionized water (4 mL) using a solvent diffusion method with gentle, precise, and continuous vertexing. Since the polymer comprises hydrophobic and hydrophilic moieties, solvent diffusion method allows the hydrophobic moieties to concentrate in the core while the hydrophilic moieties create the surface of the globular nanoparticle. This structure is stabilized through the hydrogen bond between the nanoparticle and water molecules. The drug doxorubicin is stabilized in an amphiphilic pocket

which are formed in the nanoparticle through the solvent diffusion method. The polymer resulted in carboxylic acid functionalized surface with encapsulation of doxorubicin. To make the polymer target specific for a successful cell-internalization, the surface conjugation chemistry must be modified using specific ligands. Since our target cells are a non-small cell lung cancer cells A549 which overexpresses folate receptors on the surface, the nanoparticles were conjugated with folate amine. A previously synthesized folate amine was conjugated on the surface of the nanoparticles using EDC/NHS and "Click" chemistries. After the conjugation, the drug loaded, folate conjugated, functionalized polymeric nanoparticle (PNP) was purified via dialysis technique and characterized using various techniques such as size, zeta-potential, and UV-FL.

The size of the functional PNPs were determined using a dynamic light scattering technique (DLS) shown in Figure 12, where the nanoparticle without folate amine was determined to be 78 nm in diameter and folate amine conjugated functional PNP was to be 85 nm in diameter. The size of the nanoparticle was appropriate for the cell internalization (<200 nm). The zeta-potential (surface charge) was determined using the same DLS technique where non-folate nanoparticle had -11 mV charge and folate conjugated nanoparticle had -21 mV. This change depicts a successful conjugation of folate amine on the surface of the polymer.

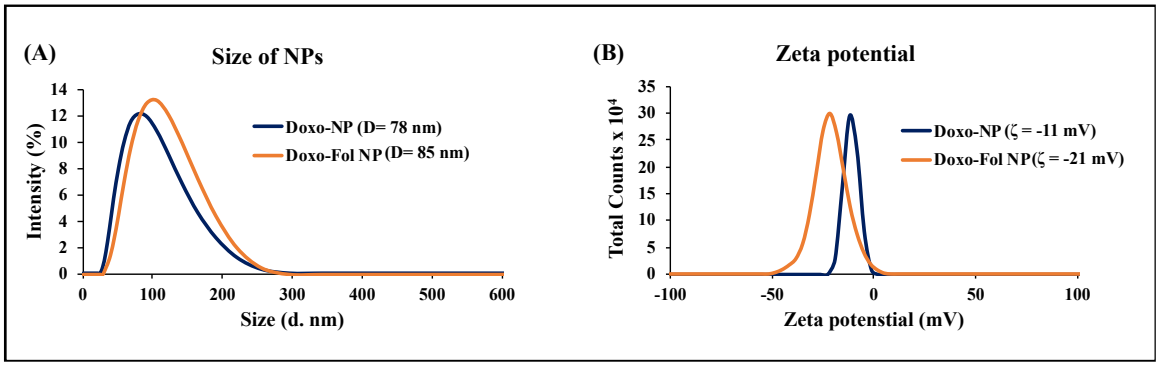

Figure 12: (A) DLS profiles of NP before and after conjugation of folic acid; (B) ζ-potential of NP before and after conjugation of folic acid.

Furthermore, the UV-FL data confirms an effective encapsulation shown in Figure 13. The non-folate nanoparticle shows the presence of Doxo at 498 nm followed by emission at 598 nm. The folate conjugated nanoparticle shows the presence of Doxo as mentioned previously and the presence of folate at 350 nm and 455 nm. These values showed not only a successful encapsulation of doxorubicin and encapsulation of folic acid but also showed stability over time. This aspect is essential for tracking the drug and its fluorescence activity while monitoring the cell-internalization process through fluorescence microscopy.

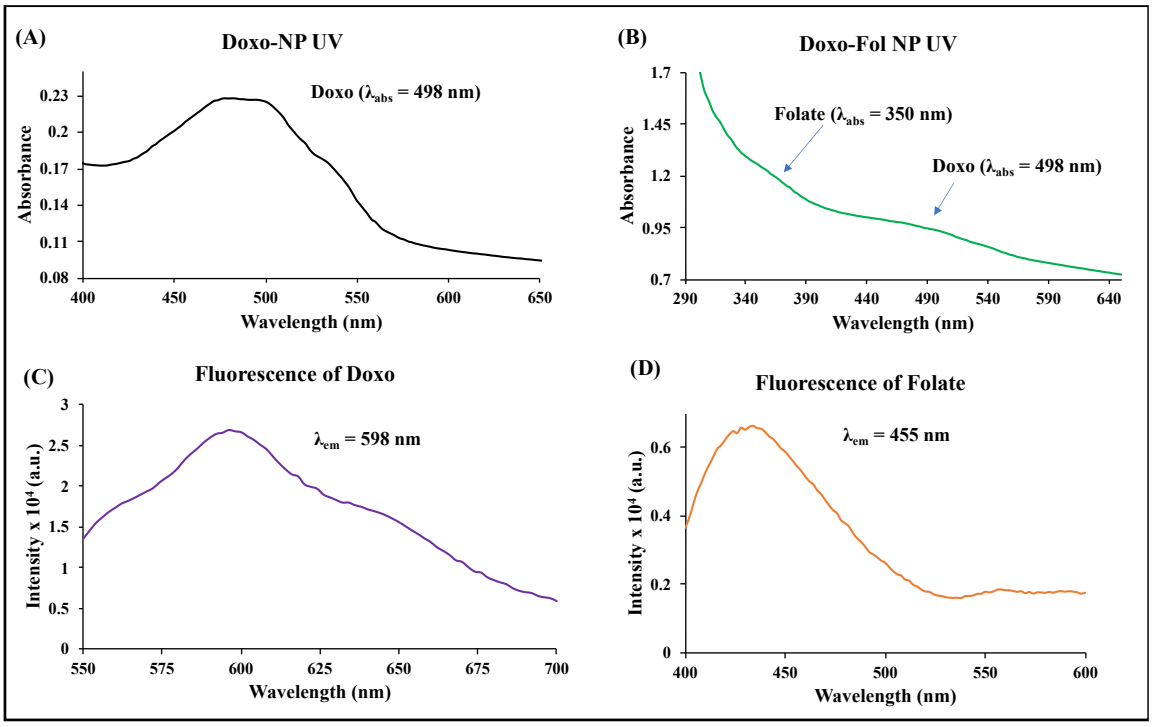

Figure 13: (A) UV-spectrum of non-folate NP with the presence of Doxo; (B) UV-spectrum of folic acid conjugated NP with the presence of Doxo; (C, D) Fluorescence spectrum of Doxo and folic acid respectively.

Cell-based in vitro experiments for targeted drug delivery:

Cell viability experiment (MTT assay):

To determine the cytotoxic efficacy of the functional PNPs, an MTT assay was performed where two types of nanoparticles were used to treat A549 lung cancer cells. The cells were seeded in. 96 well-plate for 24h at 37 °C under 5% CO_2 and incubated with folate PNP and non-folate PNP for 36h and 48h. After the incubation, the cells were treated with MTT solution and incubated for an additional 5-6 h. This additional incubation results in the formation of formazan crystals which can be analyzed by measuring an absorbance at 560 nm. MTT is metabolized by mitochondrial dehydrogenase in the healthy/alive cells, meaning that the higher the absorbance of the formazan crystals higher the cell viability. Figure 14 shows that the cells treated with folate PNP showed 5-10 % cell viability at the end of 48h whereas non-folate PNP showed 80-85 % cell viability. This indicated that conjugation of folate amine is very much target specific for the A549 cells whereas having just carboxylic acid on the surface results in very less amount of cell killing.

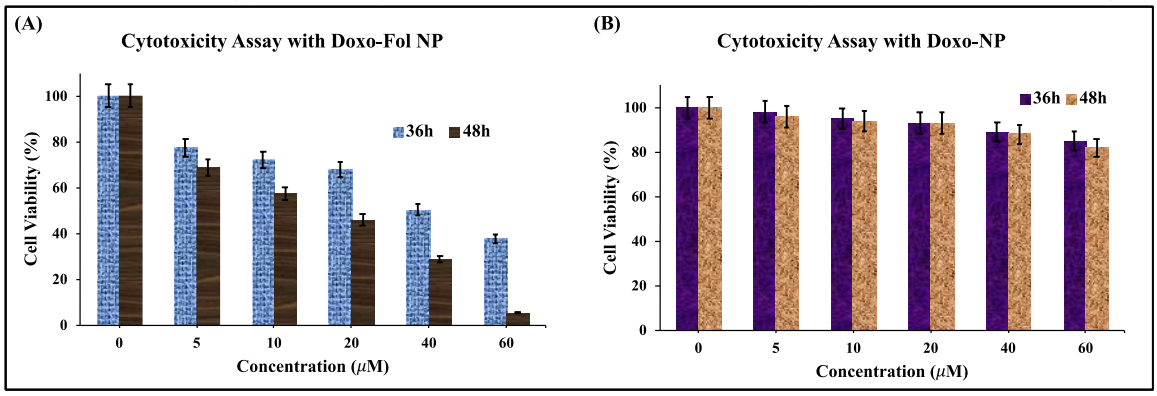

Figure 14: Cytotoxicity studies of folate conjugated and non-folate NPs on A549 cell line showed target specificity of folate-NPs.

Cellular internalization:

As proposed in our hypothesis that folate conjugated nanoparticles have a target specificity towards the folate receptor expressing tumors, a receptor-mediated and target specific internalization study was performed, and the results were evaluated using fluorescence microscopy. In this *in vitro* study, lung cancer A549 cells were seeded in a petri dish for 24 h and

incubated with folate NP for 24 h and non-folate NP for 24 and 48h under physiological conditions. A fluorescence microscopy was used to track and monitor the internalization process.

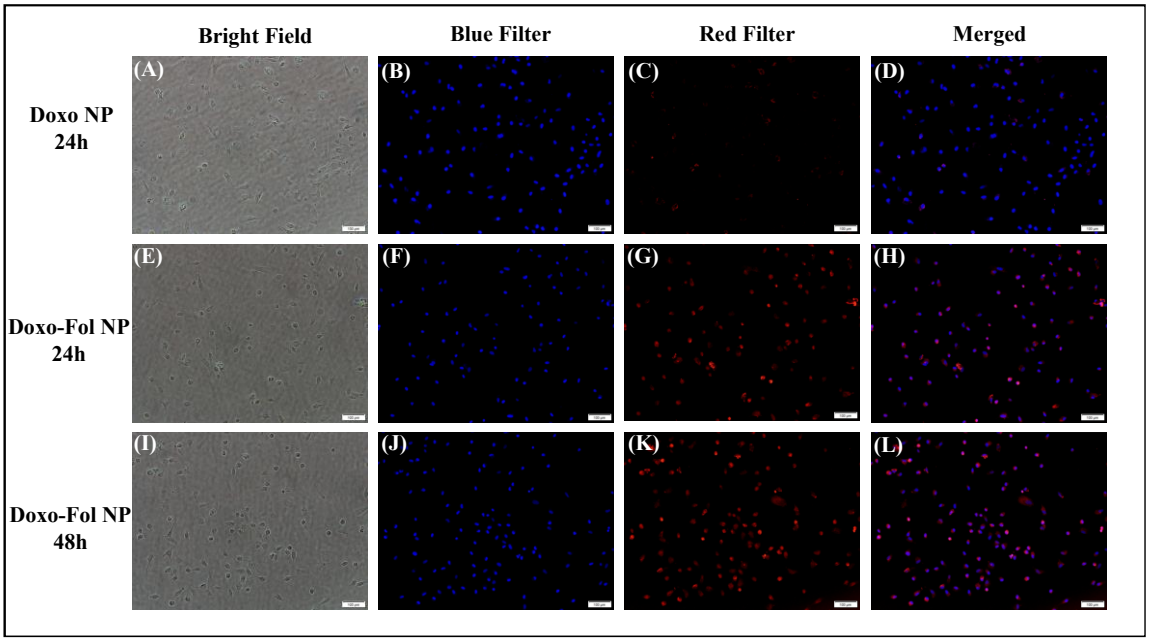

Figure 15: (A-D) Minimal cell internalization of Doxo-NPs in A549 cells; (B-H) Doxo-Fol NPs showed an effective internalization of Doxo in cytoplasm (Red dye) within 24h through folate-receptor mediated endocytosis; (I-L) Complete cell death observed in 48h by Doxo-Fol NPs where nucleus was fragmented which is stained by DAPI dye (Blue).

Our findings in Figure 15 showed that folate NP had an effective cell-internalization when observed under blue and red filter within 24h whereas there was bare minimum internalization of non-folate PNP. As the time increased, the folate NP showed fragmentation of the nucleus and cytoplasm confirming complete cell death or beyond cell death. These findings can be justified by functional group interactions. The non-folate NP has carboxylated group on the surface which interacts with folate receptors on a minimal scale. Due to lack of interaction, the internalization of the drug does not take place. On the other hand, the folate conjugated NP has folate amine on the surface that has strong affinity towards the folate receptor which results in strong interaction with A549 cells and drug can internalize successfully.

Determination of apoptotic and necrotic events:

After having results from MTT assay and cell-internalization, we wanted to determine the effect of our nanoparticles on apoptotic and necrotic process. The cells were seeded and incubated with folate NP for 24 and 48h and non-folate NP for 24h. After the incubation, the cells were treated with apoptotic dye (AnnexinV-FITC) and a necrotic dye (ethidium homodimer) to visualize and differentiate the events under fluorescence microscopy. The results in Figure 16 showed that cells treated with folate NP showed higher degree of early apoptosis and late necrosis whereas non-folate NP showed less to no fluorescence intensity. The morphology of the cells was observed in a bright field filter where apoptotic and necrotic cells had more globular structure whereas alive cells had more random shapes.

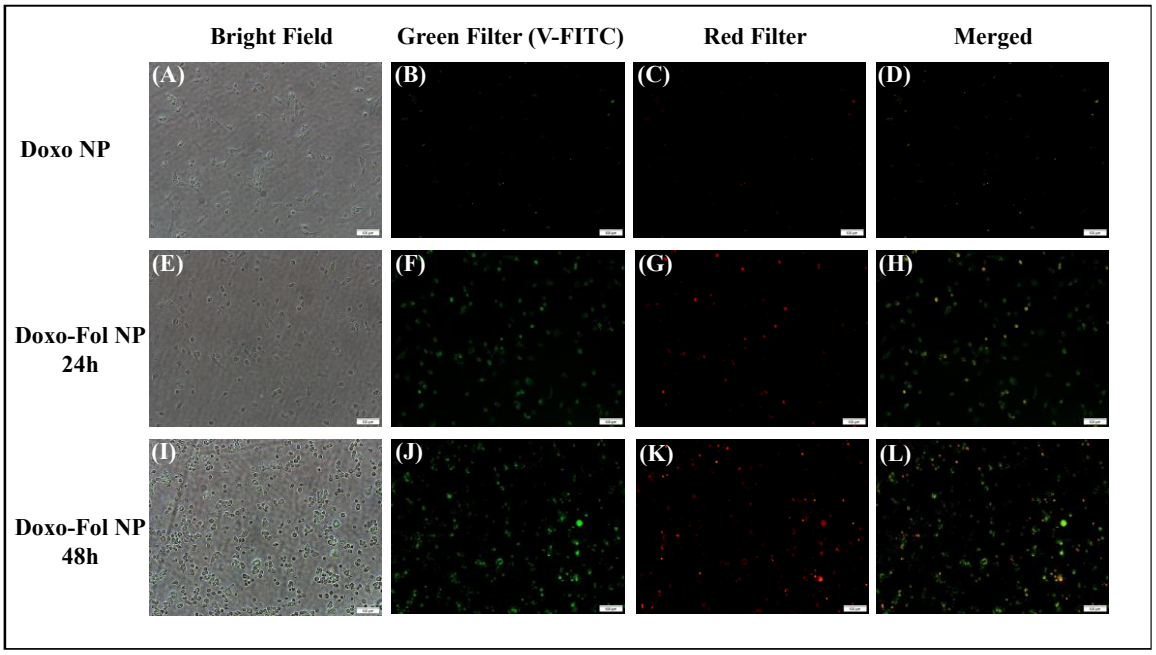

Figure 16: Determination of apoptosis and necrosis through fluorescence spectroscopy using V-FITC and ethidium homodimer III respectively. (A-D) Minimal effect of Doxo-NPs on A549 cells; (E-H) Moderate apoptotic cells within 24h treatment with Doxo-Fol NP; (I-L) Apoptotic and Necrotic cells within 48h of the treatment.

Determination of cytosolic ROS stress:

The generation of excess amounts of reactive oxygen species (ROS) have synergistic effect when it comes to cell killing. Doxorubicin is known to have a synergistic effect in the generation of the ROS so to support our hypothesis, A549 cells were treated with folate and non-folate PNP for 24 and 48h. The cells were treated with Dihydroethidium (DHE) dye for staining and to observe under fluorescence microscope. The results in Figure 17 showed that folate PNP had a synergetic effect in generating ROS whereas non-folate PNP showed minimal ROS due to lack of cell-internalization. This again confirms the target specificity of the folate conjugation.

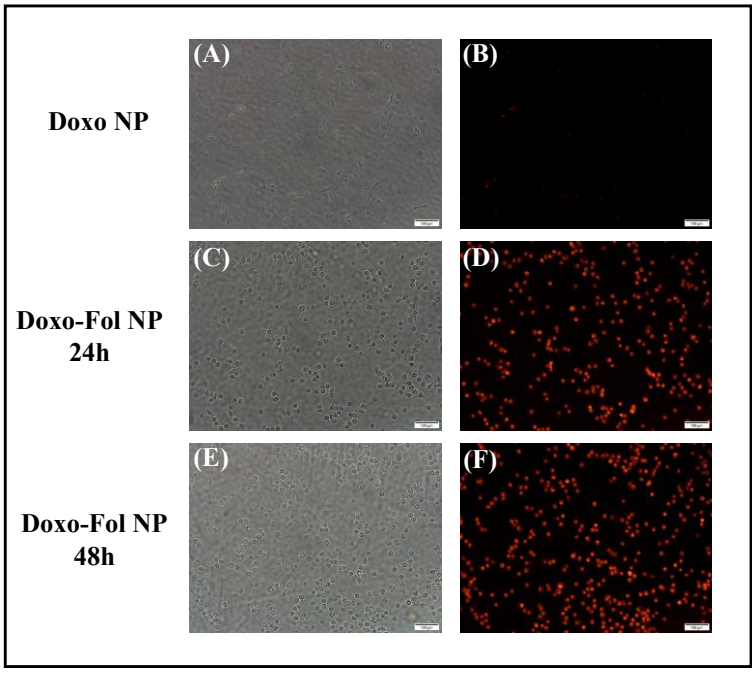

Figure 17: Fluorescence microscopy of ROS production in A549 cell line. (A, B) Minimal to no ROS production by Doxo-NPs, (C-F) relative increase in ROS production by Doxo-Fol NPs withing 48h of the treatment.

Migration and Comet assay:

To observe if our drug delivery system would arrest the metastatic activity of the cells, a migration assay was performed. The A549 cells were seeded in a 96 well-plate and incubated

with folate and non-folate PNP for 24h. A quantitative data was collected after the treatment by measuring fluorescence at 450/520 nm. The results shown in Figure 18 indicated that the cells treated with folate PNP showed least migration compared to the cells treated with non-folate PNP. The cells without any nanoparticles were treated as a control in this case.

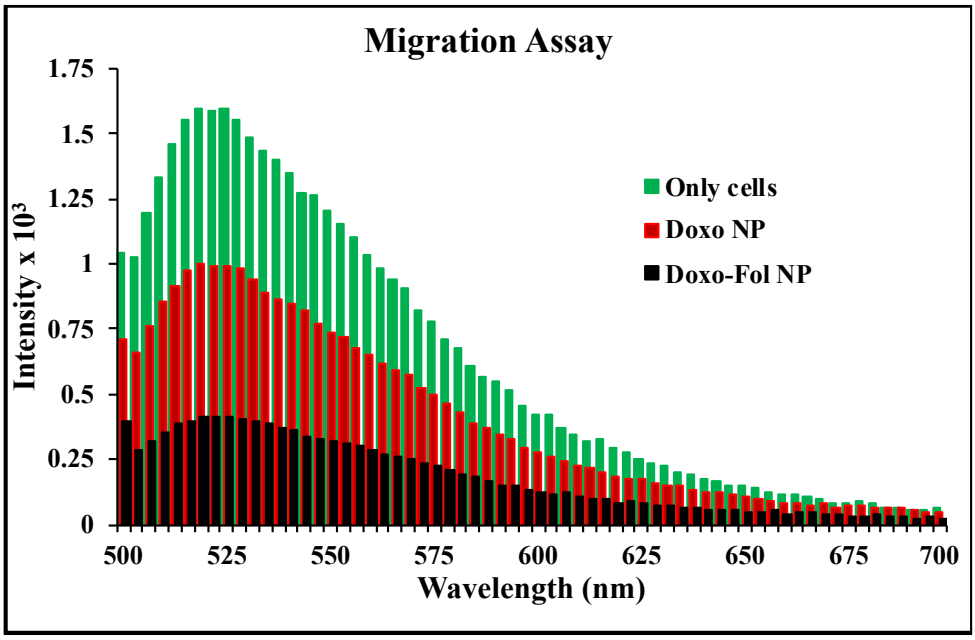

Figure 18: Evaluation of the cell lines treated with functional NPs to monitor the inhibition of migration. Results showed that A549 treated with functional NPs arrested the migration.

The comet assay was performed to observe the DNA damage in the cells. One of the exceptionally unique abilities of doxorubicin is to damage the DNA which results in a comet looking structure with a tail when observed under fluorescence microscope. The A549 cells were incubated folate and non-folate PNP for 48h and observed under fluorescence microscope. The folate PNP treated cells showed a very nice comet as shown in Figure 19 (B) whereas non-folate PNP treated cells were more oval shaped informing very less DNA damage. This confirmed that our folate PNP were more effective in destroying the DNA in the cancer cells.

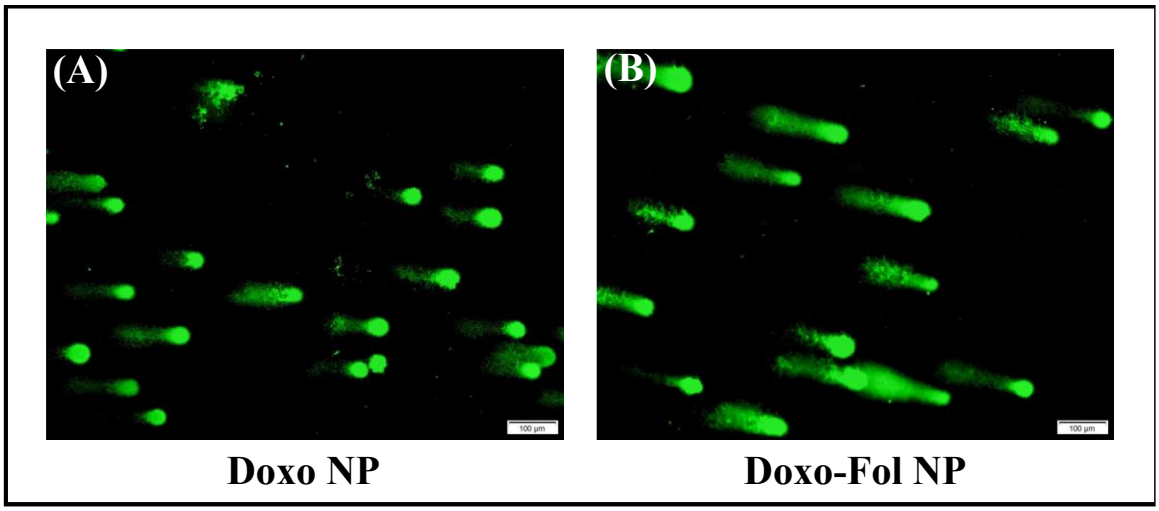

Figure 19: Comet assay using fluorescence microscopy. (A) Doxo-NPs showed minimal DNA damage which is stained with Cyber Gold Dye; (B) Doxo-Fol NPs showed comet with long tails confirming DNA damage within 48h.

Drug release study:

The drug release study allows us to determine and monitor the release of the drug in cancerous microenvironment. The drug release rate and biodegradability time are essential aspects to determine the efficacy of the designed nanoparticle system. To determine the time dependent and target specific release of the doxorubicin, the DLS technique was used using folate and non-folate PNP. Folate PNP were mimicking a tumorous microenvironment (pH 6.0) and non-folate PNP mimicked healthy microenvironment (pH 7.4). As shown in Figure 20, folate-PNP showed up to 50% release of doxorubicin within 3-4 h and went till 75-80% within 36h. The non-folate PNP showed very slow and bare minimum drug release up to 10-15% in 36h. These findings support an effective biodegradability of our drug delivery system as and confirms that non-specific drug delivery system will not result in cell killing due to less drug release.

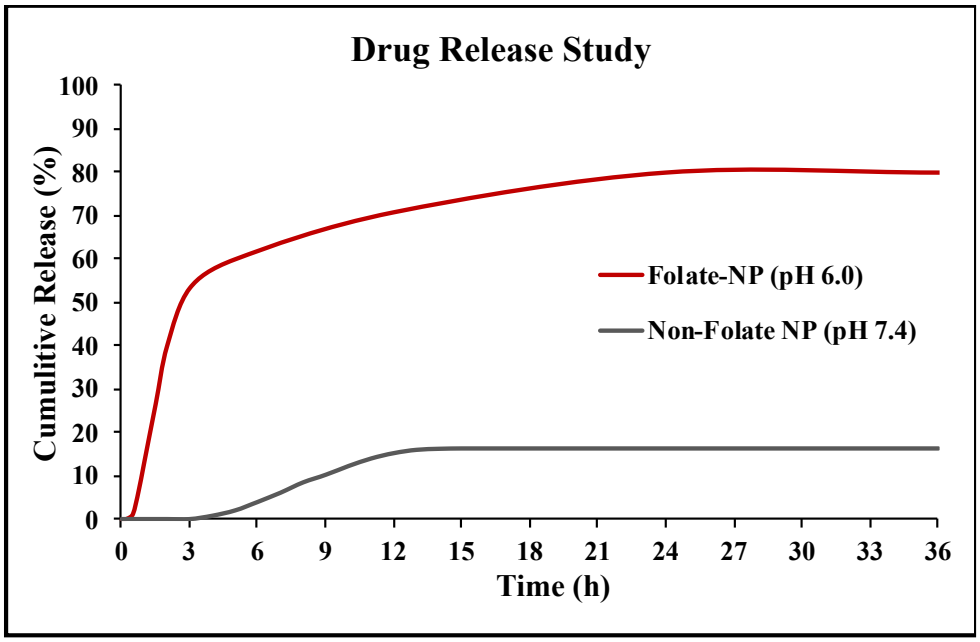

Figure 20: Cellular drug release in tumorous environment (pH 6.0) within 36h whereas minimal drug release in healthy cell environment (pH 7.4).

Chapter III

Experimental Section

Materials:

Diethyl malonate (DEM), 4-bromobutyl acetate, acetonitrile (ACN), folic acid, dimethyl sulfoxide (DMSO), tris-HCl were purchased from Sigma Aldrich and were used without any further purification. Potassium carbonate (K2CO3), sodium hydroxide (NaOH), methanol (MeOH), triethylene glycol, DTPA, p-toluenesulfonic acid (p-TSA), tetrahydrofuran (THF), trifluoroacetic acid (TFA), 10X PBS, ethylene diamine (EDA), N-hydroxysuccinamide (NHS), (1-Ethyl-3-(3-dimethylaminopropyl) carbodiimide) (EDC), MES sodium salt, Doxorubicin, 4',6-diamidino-2-phenylindole (DAPI), Isopropyl alcohol, 3-(4,5-Dimethylthiazol-2-yl)-2,5-Diphenyltetrazolium Bromide (MTT), Ethylenediaminetetraacetic acid (EDTA) were purchased from Fischer Scientific. Deuterated dimethyl sulfoxide (DMSO-d6) and chloroform (CDCl3) were purchased from Cambridge Isotope Laboratories Inc. for the 1H-NMR and 13C-NMR characterization. The matrix 2,5-dihydroxybenzoic acid (DHB) was purchased from Bruker for the MALDI-TOF mass spectroscopy. The dialysis membrane (MWCO=6-8 K) was purchased from Spectrum Laboratories. Penicillin, A549 cell line, and DMEM culture media was purchased from the American Type Culture Collection (ATCC). Cell invasion kit was purchased from Chemicon Int. Comet assay kit was purchased from Trevigen. Dihydroethidium (DHE) dye was purchased from Cayman chemicals. Fetal bovine serum (FBS) was purchased from BD Biosciences. Apoptosis and

necrosis assay kit was purchased from Biotium. Hydrogen peroxide (H2O2) and 16% paraformaldehyde were purchased from Electron microscopy science.

HBPE polymer synthesis:

Previously reported A2B monomer (1g, 5.68 mmol) and triethylene glycol (0.852g, 5.68 mmol) were added into 5 mL round bottom flask (RBF) with a stir bar, the external moisture was removed by keeping the RBF under medium vacuum for 10-15 min. Then, DTPA (0.223g, 0.568 mmol) and p-TSA (100:1 molar ratio) were added to the reaction mixture. The reaction mixture was purged 2-3 times at room temperature with a steady flow of ultra-high purity (UHP) nitrogen gas and high vacuum to remove the excess moisture from the reaction mixture. After the purging process, a steady flow of UHP nitrogen gas was supplied to the reaction while keeping the reaction in an oil bath at 140°C and slowly increasing to 176°C. Once the temperature reached 176°C, the reaction was continued under steady flow of UHP nitrogen gas for 8h. After 8h, the medium vacuum (1.5 mm/Hg) was applied for 30 min. The next step was to apply high vacuum (4 x 10^{-4} mm/Hg) to continue the polymerization for 8h at 176°C. The resulting HBPE was dissolved in DMSO and purified by precipitating in deionized water. The mixture was centrifuged, and precipitations of polymer were dissolved in methanol and dried in a vacuum oven at 45°C overnight under medium vacuum to collect final polymer. The final polymer looked amber in color and moderately viscous. The HBPE polymer was soluble in dimethyl sulfoxide (DMSO), dimethyl formaldehyde (DMF), tetrahydrofuran (THF), chloroform (CHCl3), methanol (MeOH) and insoluble in water.

Yield: 60 %, 1H NMR (300 MHz, CDCl3, *δ ppm)*: 1.21, 1.35, 1.62, 2.28, 3.44, 3.63, 4.03, 4.22. 13C NMR (300 MHz, CDCl3, *δ ppm):* 21.76, 24.51, 25.49, 28.04, 34.12, 50.59, 61.57, 64.12, 69.22,

70.59, 72.55. IR: 3426, 2932, 2867, 1729, 1457, 1346, 1165, 1106, 862, 731 cm^{-1}. TGA: 10% degradation between 265 – 270 °C.

Synthesis of Polymeric Nanoparticles:

A polymeric solution (30mg polymer in 250 µL DMSO) was obtained in a 1.5 mL Eppendorf tube. The doxorubicin (5 µL) drug was added into the polymeric solution and mixed on a vortex mixture for 15 min at 2000 rpm. The Doxo-polymer mixture was added into a 4 mL of DI water dropwise (9 µL at a time) with constant vortexing at 1500 rpm with 2 min interval between each dropwise addition. Once the Doxo-polymer mixture was added completely, the solution was kept on a tabletop mixture for 30 min. Then, the mixture was dialyzed using dialysis membrane (MWCO= 3-6 kDa) for 2-3 h in DI water. At the end of the dialysis, the solution was transferred into a new Eppendorf tube for characterization studies such as size, zeta-potential, and UV-FL. This final solution was labeled as Doxo-NP since there is no surface conjugation chemistry modified to make it target specific. This Doxo-NP serves as a negative control and can be compared with the experimental nanoparticle.

To make this nanoparticle target specific for A549 lung cancer cells, the surface conjugation chemistry must be modified with a targeting ligand folate amine. Folate amine was synthesized through EDC/NHS chemistry followed by conjugating on the surface of Doxo-NP using EDC/NHS chemistry. To synthesize folate amine, folic acid (10 mg) was dissolved in 1X PBS (8 mL, pH 7.4) in a 15 mL Eppendorf tube and kept on tabletop mixture for 15 min. A 1-Ethyl-3-(3-dimethylaminopropyl) carbodiimide (EDC) (5.5 mg in 100 µL MES buffer pH 6.0) solution was added to folic acid solution in small portions followed by N-Hydroxysuccinamide (NHS) (3.2 mg in 100 µL MES buffer pH 6.0) solution in small portions as well. The resulting mixture was given 3 minutes on a tabletop mixture and ethylene diamine (EDA) (2 µL in 100 µL DMSO) was added in 5

µL amount every 30 seconds to the parent tube. The final folate amine was stored at 4°C until further conjugation. The conjugation of folate amine on Doxo-NP was done using the "Click" chemistry. To begin with the conjugation, EDC (3 mg in 100 µL MES buffer pH 6.0) solution was added to the Doxo-NP (3 mL) in small portion with 30 second time interval and was mixed well. Then, NHS (2 mg in 100 µL MES buffer pH 6.0) solution was added to the mixture in the same pattern as EDC. The resulting mixture was mixed with hands for 3 min and synthesized folate amine (250 µL) was added to the solution (5 µL every 30 sec). The resulting mixture was placed on a tabletop mixture overnight and dialyzed using dialysis membrane (MWCO = 3-6 kDa) for 2-3 h in DI water. The final functional Doxo-Fol NP were ready for characterization studies and for the treatment of A549 cells.

Characterization:

NMR Spectroscopy: The A2B monomer, Trigol, and HBPE polymer were taken in 20-25 mg amount, vacuum dried, and dissolved in 700 µL of DMSO-d6, DMSO-d6, and CdCl3 respectively. The 1H-NMR spectra were taken using the Bruker DPX-300 MHz spectrometer and analyzed using TOPSPIN 1.3 software. Each sample was run for 100 scans with 10 second delay between each scan. The 13C-NMR spectra were taken with 30-35 mg of sample weight, vacuum dried, and dissolved in 700 µL corresponding solvent and was run for 10,000 scans using the same instrument and same program.

FT-IR: The A2B monomer, Trigol, DTPA, and polymer were vacuum dried and placed in the PerkinElmer Spectrum 2 FT-IR spectrometer in a droplet amount (1-2mg) and scanned to collect the spectra.

Differential Scanning Calorimetry (DSC): The DSC of polymer was obtained using a TA Instruments Q100 differential scanning calorimeter. A 10 mg of polymer was weighed in an aluminum bat with the lid on top and pressed to make a pallet. The device was set to -80 to 110°C temperature range with a ramp rate of 10°C/min to collect the graph.

Gel Permeation Chromatography (GPC): The GPC of the A2B monomer, trigol, and polymer was performed by vacuum drying 25 mg of the samples and dissolving into butylated hydroxytoluene (BHT)-stabilized THF (1 mL). The sample solutions were filtered through 0.2 µm filters and transferred into a GPC vial. The chromatograms were obtained using a Waters 2410 DRI gel permeation chromatograph, consisting of four phenogel 5 µL columns filled with cross-linked polystyrene-divinylbenzene (PSDVB) beads. The column was run for 38 min at 30°C at the eluent flow rate of THF of 1 mL/min.

Thermogravimetric Analysis (TGA): The TGA of polymer was performed using a TA instruments Q50 thermogravimetric analyzer. A 10 mg of polymer sample was weighed and heated under a N2 atmosphere using a ramp rate of 10°C/min for 1 h, ranging from 0-600°C.

Matrix-Assisted Laser Desorption/Ionization -Time of Flight (MALDI-TOF): To obtain MALDI-TOF spectrum of the polymer, a protocol given by the Bruker user manual was followed starting with a sample preparation to collecting and analyzing the spectra. To begin with, a TA30 solvent (30:70 volume ratio of acetonitrile in DI water to 0.1% trifluoroacetic acid) was prepared in 100 µL quantity. The matrix solution was prepared by dissolving dihydroxybenzoic acid (2mg) in TA30 solution. The polymer (5mg) was vacuum dried and dissolved in methanol (100 µL). An equal amount of polymer solution (100 µL) and TA30 solution (100 µL) was mixed well and vortexed at 850 rpm for 3 min for a complete mixing. The final mixture was placed on a MALDI target plate in a very small amount (1 µL) and the target plate was placed in a desiccator overnight under low

vacuum for the sample to dry. The instrument used for MALDI-TOF was the Bruker Microflex™ LRF MALDI-TOF. The target plate was placed in the instrument to collect the spectra and analyze it.

Dynamic Light Scattering (DLS) and Zeta Potential: The size and surface potential of the nanoparticles were measure by using the Malvern ZS90 zetasizer. The nanoparticle (10 µL) was diluted into DI water (990 µL) and the sample was placed in a standard cuvette designed for DLS reading, and gold electrode-containing cuvette for collecting zeta potential. The Zetasizer program was set to 3 runs with 35-40 sub runs each. The data were exported for plotting of DLS and zeta potential.

UV/Vis and Fluorescence Analysis: The polymeric nanoparticles (100 µL) were placed in a 96 well plate and placed in a Tecan Infinite M200 Pro microplate redear to collect the spectra. The UV/Vis absorbance of both types of nanoparticles were collected from 300-700 nm range and the fluorescence emission were collected from 400-800 nm. The readings were taken at every 3 nm interval with 10-15 flashes per reading. The final data was transferred to Microsoft Excel and graphs were plotted to observe the intensity and successful conjugation.

Cellular Based Assays/Studies:

Cell thawing and culturing: A549 cells were cultured using a BSL-2 level vacuum hood. The cells were grown in a special media containing, 89% DMEM media (1000 mL), 10% fetal bovine serum (112 mL), and 1% penicillin antibiotic (12 mL). The mixture was passed through a vacuum-filter and stored at 4°C. The cells were taken out from the liquid nitrogen storage and placed in a water bath at 37°C for 10-15 min. The cells were suspended into a 4 mL of media and centrifuged at 1000 rpm for 6 min. This resulted in the precipitation of cells at the bottom of the centrifuge tube

and formed a pallet. The cell pallet was suspended into a 4 mL of fresh, pre-warmed media. A 250 mL sterile culture flask was obtained, and the cell suspension was placed in the flask with additional 6 mL of media. The cells were grown for 24 h under 5% CO2 atmosphere at 37°C. The cells were grown until 70% confluency and were harvested and seeded again as required by the assays and studies.

Cell Internalization: A549 cells were seeded into three small petri dishes and grown until 70% confluency. The cells were treated with Doxo-NP for 24 h, Doxo-Fol NP for 24 h, and Doxo-Fol NP for 48 h and incubated under 5% CO2 atmosphere at 37°C. After the treatment time, the cells were washed twice with 1X PBS (pH 7.4) and fixed using 4% paraformaldehyde solution for 15 min at room temperature in the dark. The washing process with 1X PBS was repeated and cells were stained using 6-diamidino-2-phenylindole (DAPI, 5 mg/mL) dye for 15 min at room temperature in the dark. The cells were washed and stored with 1X PBS for the fluorescence microscopy images taken by Olympus IX73 microscope.

Cytotoxicity studies using MTT assay: The A549 cells were seeded into a 96 well plate and grown for 24 h. To determine the potential dose-dependent and time-dependent cytotoxicity, Doxo-NP and Doxo-Fol NP were used in different dosage starting from 0, 5, 10, 20, 40, and 60 µL and treated for 36 h and 48 h in the incubator. After the treatment time, cells were incubated with 30 µL of MTT solution (5mg MTT in 1 mL 1X PBS) for 6 h which resulted in the formation of purple formazan crystals. The crystals were dissolved in 75 µL of acidic isopropanol (10 mL isopropanol in 250 µL concentrated HCl). The absorbance of the crystals was recorded at 570 nm using a TECAN microplate redear.

Reactive Oxygen Species (ROS) Studies: A549 cells were seeded and grown into three small petri dishes. The cells were treated with Doxo-NP for 24 h, Doxo-Fol NP for 24 h and 48 h in the incubator. After the treatment, the cells were washed twice with 1X PBS and stained with 20 µL of DHE dye for 30 min at room temperature in the dark. Then, the cells were washed with 1X PBS again and fixed using 4% paraformaldehyde for 15 min at room temperature in the dark. The cells were washed and stored in 1X PBS for the fluorescence microscopy using Olympus IX73.

Apoptosis and Necrosis Assay: The A549 cells were seeded in three small petri dishes and treated with Doxo-NP for 24 h, Doxo-Fol NP for 24 and 48h in the incubator. After the treatment, cells were washed with 1X PBS. A 1X Binding Buffer was prepared by diluting 5X Annexin V Binding Buffer with dH2O. A staining solution was prepared using 1X Binding Buffer (100 µL), FITC Annexin V (5 µL), and ETHD-III (5 µL). The cells were treated with staining solution for 15 min at room temperature in the dark. The cells were washed with 1X PBS and fixed using 4% paraformaldehyde for 15 min in the dark. The cells were washed and stored in 1X PBS for fluorescence microscopy using Olympus IX73.

Cell Invasion Assay: To determine the efficacy of the drug delivery system in stopping migration of the cells from one place to other, migration assay was performed using QCM™ 96-Well Cell Invasion Kit from CHEMICON Int. The cells were harvested and suspended into a serum free media. The insert tray was rehydrated using serum free media for 1-2 h and the media was removed at the end of rehydration. A 150 µL of serum free media was placed into a feeder tray and the insert tray was submerged in the feeder tray. A 100 µL of cell suspension was placed in the insert and cells were treated with 1X PBS (60 µL), Doxo-NP (60 µL), Doxo-Fol NP (60 µL) for 24 h in the incubator. The treatment time allows the starved cells to invade the collagen layer. The migrated cells were detached using detachment buffer (200 µL) for 30 min and collected into a

new 96 well plate for staining. The staining solution was prepared by diluting CyQuant GR Dye 1;75 with 4X Lysis Buffer. A 150 µL of staining solution was placed to stain the cells and incubated for 15 min at room temperature. The fluorescence reading was taken at 480/520 nm using TECAN infinite M200 Pro microplate redear.

Drug Release Studies: To determine the efficiency of the drug delivery system, an in vitro drug release study was performed. Doxo-NP (200 µL) was placed in a dialysis cup and incubated in 1X PBS (pH 7.4) for 36 h. The Doxo-Fol NP (200 µL) was placed in a dialysis cup with 50 µL 1X PBS (pH 4.0) and incubated in 1X PBS (pH 7.4) for 36 h. Throughout the time, 1 mL aliquots from PBS were taken and fluorescence emission was measured at 494 nm. A standard calibration curve was made to calculate the concentration of released drug using the following formula. Cumulative release (%) = $(guest)_t/(guest)_{total}$ X 100.

Comet Assay: A549 cells were seeded and treated with Doxo-NP and Doxo-Fol NP for 48 h. The cells were trypsinized and centrifuged at 1000 rpm for 6 min to form a pallet. The cell pallet was resuspended in 1X PBS (pH 7.4) and mixed with low-melt agarose gel in 1:10 ratio. The mixture was placed on comet slides and the slide was kept at 4°C for 30 min and immersed in lysis solution for 45 min at 4°C in the dark. The slide was later then submerged into an alkaline unwinding buffer (pH >13) for 1 h, at 4°C in the dark. The electrophoresis was carried out at 4°C for 30 min at 21V. The slides were rinsed and submerged in DI water for 5 min followed by submerging in 70% ethanol for 5 min. The staining of the gel was done using SYBR Gold solution for 30 min at room temperature in the dark and the slides were rinsed with DI water and kept at 37°C to dry. The fluorescence microscopic images were taken using FITC filter on Olympus IX73.

Chapter IV

Conclusion

A novel hyperbranched polyester was successfully synthesized from our proprietary A_2B monomer, triethylene glycol and DTPA. The resulting HBPE showed promising characterization through NMR, GPC, MALDI-TOF, TGA, etc. for the biological applications in targeted therapy of A549 lung cancer cells. The polymer was turned into a nanoparticle encapsulating anti-cancer drug doxorubicin. The surface functionality of HBPE allowed a successful conjugation of a ligand which is target specific for the A549 cell line. The nanoparticle suspensions were characterized using DLS, zeta potential, and UV-FL to continue in vitro studies. The cellular assays such as cell internalization, apoptosis and necrosis, ROS studies, cytotoxicity studies (MTT), migration studies, drug release, and comet assay showed overall 80-85% cell death in 48 of incubation with Doxo-Fol NP while Doxo-NP had minimum effect which supports the hypothesis of this research.

To continue this research in future, an incorporation of gadolinium with DTPA would provide a platform to monitor a MR imaging where T1 and T2 relaxation can be recorded which helps in monitoring the treatment of cancer.

References

(1) Siegel, R. L.; Miller, K. D.; Fuchs, H. E.; Jemal, A. Cancer Statistics, 2022. *CA: A Cancer Journal for Clinicians* 2022, *72* (1), 7–33. https://doi.org/10.3322/CAAC.21708.

(2) SCLC vs. NSCLC: What's the Difference? | NFCR Lung Cancer Awareness https://www.nfcr.org/blog/small-cell-lung-cancer-vs-non-small-cell-lung-cancer-whats-the-difference/ (accessed 2022 -04 -05).

(3) Cho, K.; Wang, X.; Nie, S.; Chen, Z.; Shin, D. M. Therapeutic Nanoparticles for Drug Delivery in Cancer. *Clinical Cancer Research* 2008, *14* (5), 1310–1316. https://doi.org/10.1158/1078-0432.CCR-07-1441.

(4) Burford, R.; Emeritus, F. Polymers: A Historical Perspective. *Journal & Proceedings of the Royal Society of New South Wales* 2019, *152* (2), 242–250.

(5) Polymer Definition & Meaning - Merriam-Webster https://www.merriam-webster.com/dictionary/polymer (accessed 2022 -04 -05).

(6) Staudinger, H. THE FOUNDATION OF POLYMER SCIENCE BY. 1999.

(7) Linear Polymer - an overview | ScienceDirect Topics https://www.sciencedirect.com/topics/engineering/linear-polymer (accessed 2022 -04 -05).

(8) Aboudi, K.; Ahmed, B.; Tyagi, V. K.; van Lier, J. B. Occurrence and Fate of Aromaticity Driven Recalcitrance in Anaerobic Treatment of Wastewater and Organic Solid Wastes. *Clean Energy and Resources Recovery* 2021, 203–226. https://doi.org/10.1016/B978-0-323-85223-4.00025-7.

(9) Classification of Polymers - GeeksforGeeks https://www.geeksforgeeks.org/classification-of-polymers/ (accessed 2022 -04 -05).

(10) Polymers: an overview https://www.essentialchemicalindustry.org/polymers/polymers-an-overview.html (accessed 2022 -04 -05).

(11) Langer, R.; Brem, H.; Tapper, D. Biocompatibility of Polymeric Delivery Systems for Macromolecules. *Journal of Biomedical Materials Research* 1981, *15* (2), 267–277. https://doi.org/10.1002/JBM.820150212.

(12) Appel, E. A.; Tibbitt, M. W.; Webber, M. J.; Mattix, B. A.; Veiseh, O.; Langer, R. Self-Assembled Hydrogels Utilizing Polymer-Nanoparticle Interactions. *Nat Commun* 2015, *6*. https://doi.org/10.1038/NCOMMS7295.

(13) Ma, S.; Xu, Y.; Song, W. Functional Bionanomaterials for Cell Surface Engineering in Cancer Immunotherapy. *APL Bioengineering* 2021, *5* (2), 021506. https://doi.org/10.1063/5.0045945.

(14) Knop, K.; Hoogenboom, R.; Fischer, D.; Schubert, U. S. Poly(Ethylene Glycol) in Drug Delivery: Pros and Cons as Well as Potential Alternatives. *Angew Chem Int Ed Engl* 2010, *49* (36), 6288–6308. https://doi.org/10.1002/ANIE.200902672.

(15) Chereddy, K. K.; Vandermeulen, G.; Préat, V. PLGA Based Drug Delivery Systems: Promising Carriers for Wound Healing Activity. *Wound Repair Regen* 2016, *24* (2), 223–236. https://doi.org/10.1111/WRR.12404.

(16) Ma, Y.; Mou, Q.; Wang, D.; Zhu, X.; Yan, D. Dendritic Polymers for Theranostics. *Theranostics* 2016, *6* (7), 930. https://doi.org/10.7150/THNO.14855.

(17) Santra, S.; Kumar, A. Facile Synthesis of Aliphatic Hyperbranched Polyesters Based on Diethyl Malonate and Their Irreversible Molecular Encapsulation{ Scheme 1 Synthesis of Aliphatic HBPEs from AB 3 and AB 2 Monomers. 2004. https://doi.org/10.1039/b404447a.

(18) Santra, S.; Kaittanis, C.; Manuel Perez, J. Aliphatic Hyperbranched Polyester: A New Building Block in the Construction of Multifunctional Nanoparticles and Nanocomposites. *Langmuir* 2010, *26* (8), 5364–5373. https://doi.org/10.1021/la9037843.

(19) Madaan, K.; Kumar, S.; Poonia, N.; Lather, V.; Pandita, D. Dendrimers in Drug Delivery and Targeting: Drug-Dendrimer Interactions and Toxicity Issues. *Journal of Pharmacy & Bioallied Sciences* 2014, *6* (3), 139. https://doi.org/10.4103/0975-7406.130965.

(20) Dendrimers https://polymerdatabase.com/polymer%20chemistry/Dendrimers2.html (accessed 2022 -04 -05).

(21) Khan, I.; Saeed, K.; Khan, I. Nanoparticles: Properties, Applications and Toxicities. *Arabian Journal of Chemistry* 2019, *12* (7), 908–931. https://doi.org/10.1016/J.ARABJC.2017.05.011.

(22) Laurent, S.; Forge, D.; Port, M.; Roch, A.; Robic, C.; vander Elst, L.; Muller, R. N. Magnetic Iron Oxide Nanoparticles: Synthesis, Stabilization, Vectorization, Physicochemical Characterizations, and Biological Applications. *Chemical Reviews* 2009, *110* (4), 2574. https://doi.org/10.1021/CR900197G.

(23) Abedi-Gaballu, F.; Dehghan, G.; Ghaffari, M.; Yekta, R.; Abbaspour-Ravasjani, S.; Baradaran, B.; Ezzati Nazhad Dolatabadi, J.; Hamblin, M. R. PAMAM Dendrimers as Efficient Drug and Gene Delivery Nanosystems for Cancer Therapy. *Applied Materials Today* 2018, *12*, 177–190. https://doi.org/10.1016/J.APMT.2018.05.002.

(24) Dreaden, E. C.; Alkilany, A. M.; Huang, X.; Murphy, C. J.; El-Sayed, M. A. The Golden Age: Gold Nanoparticles for Biomedicine. *Chemical Society Reviews* 2012, *41* (7), 2740–2779. https://doi.org/10.1039/C1CS15237H.

(25) Shin, W. K.; Cho, J.; Kannan, A. G.; Lee, Y. S.; Kim, D. W. Cross-Linked Composite Gel Polymer Electrolyte Using Mesoporous Methacrylate-Functionalized SiO2 Nanoparticles for Lithium-Ion Polymer Batteries. *Scientific Reports 2016 6:1* 2016, *6* (1), 1–10. https://doi.org/10.1038/srep26332.

(26) Naz, S.; Beach, J.; Heckert, B.; Tummala, T.; Pashchenko, O.; Banerjee, T.; Santra, S. Cerium Oxide Nanoparticles: A "radical" Approach to Neurodegenerative Disease Treatment. *Nanomedicine (Lond)* 2017, *12* (5), 545–553. https://doi.org/10.2217/NNM-2016-0399.

(27) Alnasser, R.; Shaw, Z.; Santra, S. Hyperstar Polyester-Based Functional Nanotheranostics for the Targeted Drug Delivery and Treatment of Cancer. 2019. https://doi.org/10.1002/cnma.201900517.

(28) Biomaterials Science Rsc.Li/Biomaterials-Science. 2020. https://doi.org/10.1039/c9bm01475f.

(29) Jain, V.; Shelby, T.; Patel, T.; Mekhedov, E.; Petersen, J. D.; Zimmerberg, J.; Ranaweera, A.; Weliky, D. P.; Dandawate, P.; Anant, S.; Sulthana, S.; Vasquez, Y.; Banerjee, T.; Santra, S. A Bimodal Nanosensor for Probing Influenza Fusion Protein Activity Using Magnetic Relaxation. 1899, *6*. https://doi.org/10.1021/acssensors.1c00253.

(30) Higashihara, T.; Segawa, Y.; Sinananwanich, W.; Ueda, M. Synthesis of Hyperbranched Polymers with Controlled Degree of Branching. *Polymer Journal 2012 44:1* 2011, *44* (1), 14–29. https://doi.org/10.1038/pj.2011.99.

(31) Mitchell, M. J.; Billingsley, M. M.; Haley, R. M.; Wechsler, M. E.; Peppas, N. A.; Langer, R. Engineering Precision Nanoparticles for Drug Delivery. *Nature Reviews Drug Discovery 2020 20:2* 2020, *20* (2), 101–124. https://doi.org/10.1038/s41573-020-0090-8.